Published in Journal of Structural Geology 21, issues 8-9, 1089-1101, 1999,
which should be used for any reference to this work

Strain, displacement and rotation associated with the formation of curvature in fold belts; the example of the Jura arc

David Hindle [1], Martin Burkhard*

Institut de Géologie, rue E. Argand 11, CH 2000 Neuchâtel, Switzerland

Abstract

A new simplified genetic classification scheme for arcuate fold–thrust belts is proposed. Based on total strain patterns and displacement vector fields, we distinguish three extreme end-member models: (1) 'Oroclines', pure bending of an initially straight belt, (2) 'Piedmont glacier' with divergent transport directions and (3) 'Primary arcs'. A simple geometric model set-up for the simulation of strain patterns in primary arcs with uniform transport direction demonstrates that divergent strain trajectories and rotations of passive marker lines do not require any divergence in displacement directions. These often quoted arguments are insufficient for the identification of 'Oroclinal bending' or 'Piedmont glacier' type of arc formation. Only three-dimensional restorations of an arc provide the critical information about displacement directions. In their absence, arc parallel stretches and rotations in comparison with total strains provide the most useful criteria for the distinction of arc formation modes. As an example, the Jura fold–thrust belt of the external Alps is discussed. A large set of strain data includes total shortening estimates based on balanced cross-sections, local strain axes orientations from the inversion of fault populations [Homberg, C., 1996. Unpublished PhD thesis, Université de Paris VI (France)], tectonic stylolites and micro-strains from twinning in sparry calcite. Strain trajectories (maximum shortening direction) computed from these data define a strongly divergent fan with a 90° opening. A complete displacement vector field for the entire Jura has been determined from balanced cross-sections augmented with three-dimensional 'block mosaic' restorations [Philippe, Y., 1995. Unpublished PhD thesis, Université de Chambéry (France)]. Displacement vectors diverge by about 40°, markedly less than strain trajectories. The non-parallelism between strain trajectories and transport directions indicates that considerable wrenching deformation did occur in both limbs of the Jura arc. Paleomagnetically determined clockwise rotations of 0–13° from ten sites (Kempf, O., et al., Terra Nova 10, 6–10) behind the right-hand half of the Jura arc and two sites with a combined 23° anticlockwise rotation behind the left-hand half of the arc are and additional argument in favor of such a wrenching deformation. We conclude that the Jura arc formed as a 'Primary arc' with a minor component of 'Piedmont glacier' type divergence in transport directions.

1. Introduction

Arcuate mountain belts range in scale from tens of kilometers in thin-skinned foreland fold–thrust belts (Marshak, 1988) up to hundreds of kilometers, where the entire crust or lithosphere is involved (Isacks, 1988). Seen from the foreland side, arcuate folding patterns strongly suggest radial spreading of material (Argand, 1924; Platt et al., 1989). Considering the concave side of an arc, however, spreading models are faced with severe space problems because the same area in the center of the arc is claimed as a source region to large amounts of material, which supposedly moved in divergent directions. Despite their widespread occurrence along compressional plate boundaries few if any examples exist where the arc forming processes are well documented and understood (Wezel, 1986). We simplify and modify existing classification

* Corresponding author.
E-mail address: martin.burkhard@geol.unine.ch (M. Burkhard)
[1] Present address: Shell International Exploration and Production, Research and Technical Services EPT-HM, Vomerlaan 8, PO Box 60, 2280AB Rijswijk, The Netherlands.

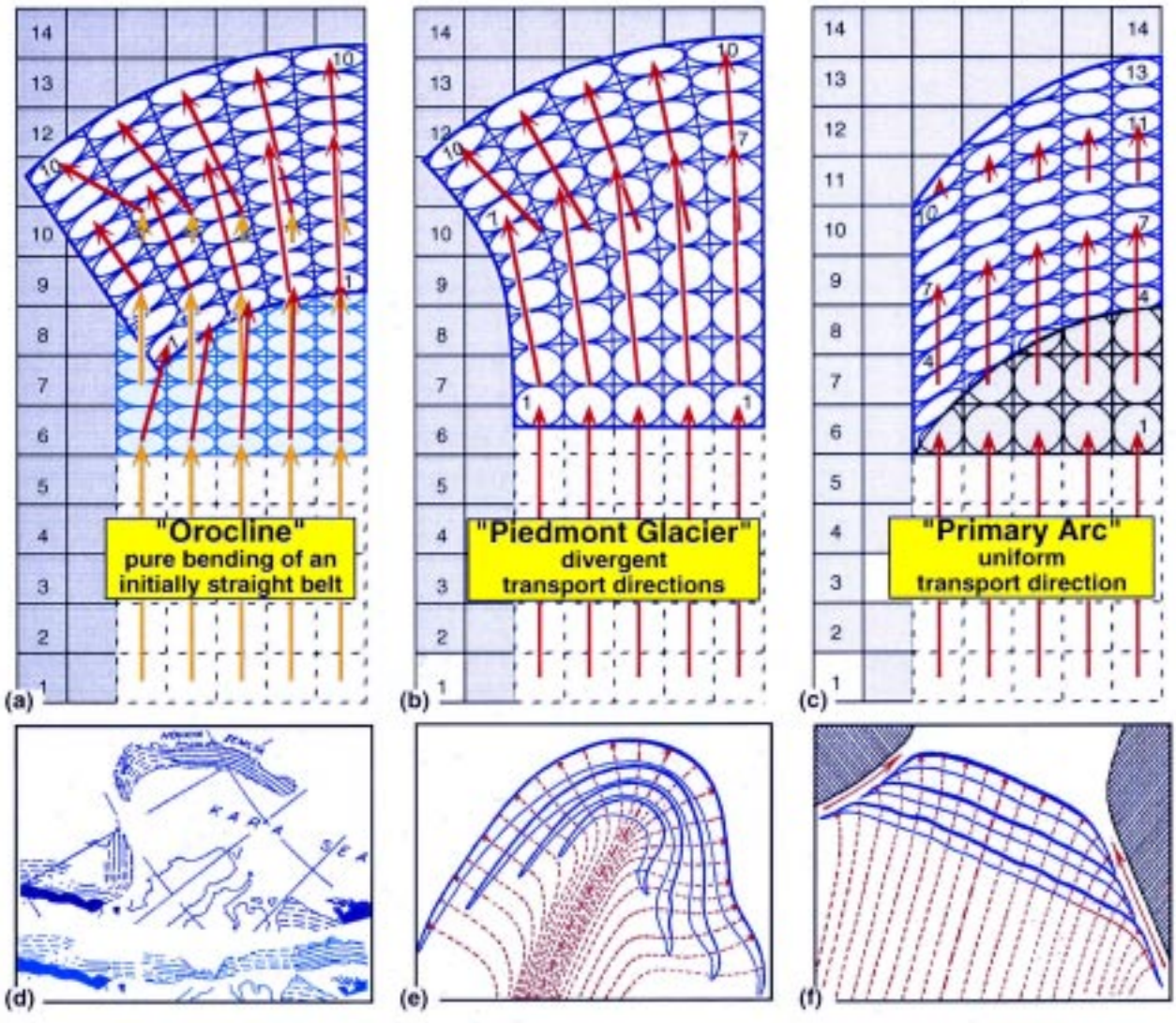

Fig. 1. Conceptual arc formation models. Strains and rotations in map view are illustrated using an initially square grid and finite strain ellipses (in blue). Undeformed Foreland is shaded in grey. Some grid positions are numbered for comparison with the deformed grid within the arcs. Finite displacement vectors in red are superimposed for grid lines 1, 7 and 10. (a) Orocline model: according to Carey (1955), an initially straight belt is bent into an arc shape during a second stage of deformation, modeled here as a pure bending. (b) 'Piedmont glacier' model with strongly divergent displacement directions. (c) 'Primary arc' with uniform transport direction. (d) The Novaya Zemlya arc formation in two steps according to Carey (1955, details from his figs. 15 and 16). (e) Modified detail from the schematic fig. 2 of Argand (1924) showing a 'virgation du premier genre'. (f) Modified detail from the schematic fig. 4 of Argand (1924) showing a 'virgation du deuxième genre'.

schemes (Marshak, 1988; Ferrill, 1991; Ferrill and Groshong ,1993) and concentrate on three extreme end members in Fig. 1: (A) Oroclinal bending, (B) 'Piedmont glacier' and (C) 'Primary arc'. This conceptual and genetic classification puts the emphasis on the complete displacement vector field and resulting total strain patterns. These key parameters are portrayed in Fig. 1 with the aid of a strain grid and strain ellipses for internal bulk deformations, rotations and structural trends. Although such a classification seems straightforward in principle, geologists are confronted with the inverse problem. Based on the structural grain in a mountain belt as seen in a satellite picture or tectonic map, strain determinations from balanced cross-sections, maybe completed with some paleomagnetic data for rotations, we try to reconstruct the total displacement vector field of an arc. With such quite incomplete data-bases, it is questionable if we are ever able to distinguish the subtle differences which exist between the displacement vector fields of up to eight different arc formation modes proposed by Marshak (1988, fig. 6). Here we try the less ambitious task to establish criteria for the distinction of only three end-member cases.

Based on a simple model set-up of a primary arc, we examine the complex relationships between strain,

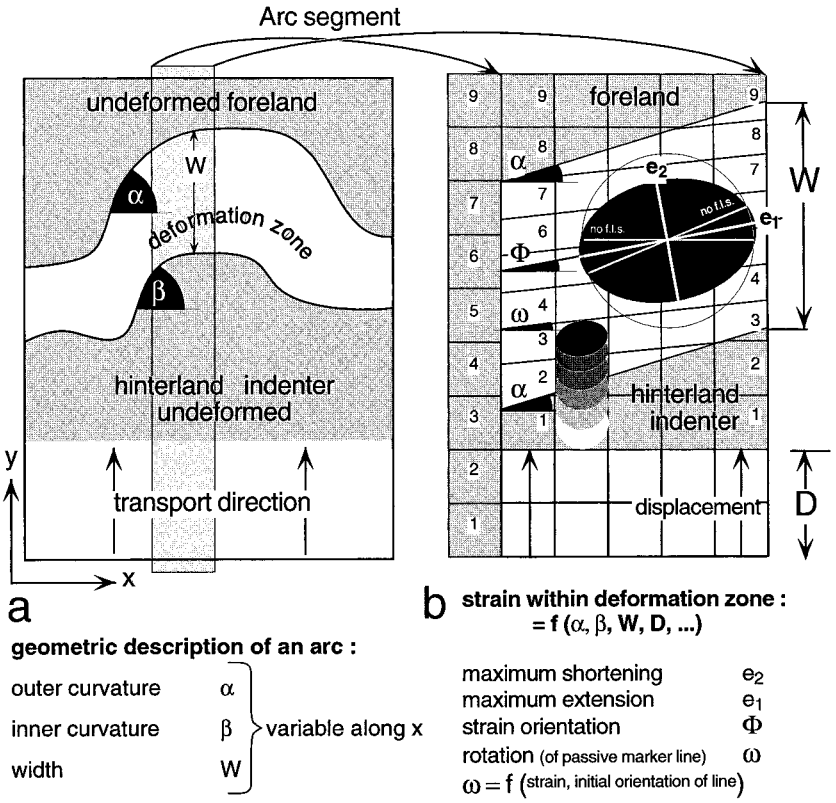

Fig. 2. Primary arc model with uniform displacement direction. (a) Schematic arcuate deformation zone and definitions of some geometric parameters used for the modeling of strains within a segment of this oblique deformation zone. (b) Model set-up of a segment of an arcuate deformation zone, used to investigate the relationships between finite strain, displacement and curvature. Letters describing various lengths and angles are used for calculation of strain parameters in Fig. 3 and discussion in main text.

rotation and displacement in oblique deformation zones. Simple geometric modeling shows indeed that neither fanning strain trajectories, nor rotations about vertical axes, nor arc-parallel extensions are sufficient arguments for a divergence in material flow. The difficulties in distinguishing arc formation modes are discussed for the case of the Jura fold–thrust belt. There are probably few if any other arcs in the world with more strain data, and still, there remains considerable uncertainty about the arc formation mechanisms responsible for the formation of this late alpine arcuate fold–thrust belt.

2. Arc formation models

In the 'orocline' according to the concept of Carey (1955), the arcuate shape of a mountain belt is achieved in two steps: an initially straight fold–thrust belt is bent into an arc during a second deformation event, e.g. when such a belt is molded onto an irregularly shaped continental margin or other 'basement' obstacle during final stages of collision. In Fig. 1(a), this sequence of events is sketched by a first pure shear shortening (light blue ellipses) followed by a second event of pure bending. The resulting finite strain pattern is illustrated by superimposed dark blue ellipses. Although Carey (1955) did not elaborate on the possible mechanisms of bending the first straight belt into a curved one, the 'orocline concept' is most often used to infer a pure bending. Such an 'orocline' in the restricted sense is characterized by arc-parallel extension on the outer side and arc-parallel compression on the inner side of the arc. As shown in Fig. 1(a), strain incompatibilities both in the foreland and the hinterland of the orocline are large. In particular, shortening in a general direction perpendicular to the symmetry axis of the arc would be expected on the inner side. This shortening increases with the rotation of the two limbs of the arc. Passive rotations of these limbs are equal to their angle with the supposedly straight line they formed prior to oroclinal bending. Such rotations around vertical axes are directly quantified with paleomagnetic methods (Eldredge et al., 1985; Lowrie and Hirt, 1986; Isacks, 1988; Tait et al., 1996) and the term 'oroclinal bending' is most often used in the context of paleomagnetically determined 'rigid block' rotations in an arcuate fold belt. Limb rotation alone is not a sufficient argument for the identification of pure 'oroclinal bending', since substantial rotations also occur from

other arc formation modes such as differential transport to the foreland (Marshak et al., 1992, figs. 1–3) and/or shortening deformation within an oblique zone as shown (Fig. 1c and Fig. 2). The Bolivian Andes as one of the classic paleomagnetically 'documented' examples of oroclinal bending has convincingly been reinterpreted by Sheffels (1995) as a 'primary arc'.

The 'Piedmont glacier' model of 'radial thrusting/spreading' (Fig. 1b) (Merle, 1989), requires a clear separation of an arcuate fold nappe emplaced upon an undeformed foreland. Nappe internal strains are characterized by foreland-ward increasing arc-parallel extensions. Along radially divergent transport- ('flow'-) directions, strains may vary from extensional at the rear to compressional at the front. As in the oroclinal bending model, passive rotations of initially straight marker lines in the arc's limbs are as large as suggested by the curved outline of the 'spreading' arc. Radial thrusting/spreading is probably the most popular type of arc formation model ever since Argand's 'La Tectonic de l'Asie' (Argand, 1924, p. 207ff and fig. 2) where his drawings clearly show such 'virgations du premier genre' to be responsible for almost any arcuate belt in the Alpine–Himalayan chain (op. cit. figs. 9 and 10).

The 'primary arc' is a fold–thrust belt which adopts an arcuate shape right from the beginning of its formation. Such a curvature in the thrust front of a foreland fold–thrust belt may be induced by a series of boundary conditions. Lateral variations in facies, thickness, layering in the hanging wall and/or irregularities in the footwall/foreland are all potential sources for the generation of curvature in fold–thrust belts (Marshak et al., 1992). A very simple geometric model of an idealized primary arc is shown in Fig. 1(c). This model set-up demonstrates that an arcuate deformation belt can even be produced in an environment of rigorously uniform displacement direction (Ferrill, 1991). The consumption of the advance of an arcuate indenter within a curved deformation zone, i.e. a primary arc, leads necessarily to divergent, fanning strain trajectories within this deformation zone. The limbs of any arc produced in this way are characterized by transpressional wrenching deformation (Sanderson and Marchini, 1984; Sylvester, 1988; Marshak et al., 1992; Wilkerson et al., 1992). Argand (1924, p. 210 and fig. 4) called this mechanism 'virgation du deuxième genre' and clearly considered it of lesser importance.

The key parameter used in distinction of arc types, namely the displacement vector field, is the most difficult to obtain in nature. This explains why so many different arc classification schemes have been proposed in the past. Critical examination of the three end-member models portrayed in Fig. 1 shows that it may even be difficult to distinguish between three extreme arc formation models of Fig. 1 if only the central, frontal portions of an arc are considered. All models involve rotations of passive marker lines as well as strike-parallel extensions within the limbs of the arc. Large strike-parallel extensions in the frontal parts of the arc are a strong argument in favor of either oroclinal bending or divergent thrusting/spreading. Regarding rotations, however, only the precise angles of rotation in relation with the strike of the arc's limbs, and total strain provide a sufficient criterion to discriminate the 'primary arc' from the other two models (Eldredge et al., 1985). Ideally, the total strain distribution or at least gradients in extensional strains across and along strike should be known, because this is the only way to determine the displacement directions in various parts of an arc.

3. Modeling strains in a 'primary arc' with uniform transport direction

A simple geometric two-dimensional model has been designed in order to evaluate the relationships between displacement vector fields, arc shape and finite strain axes orientations in variations of a primary arc model (Fig. 2a). In this conceptual model set-up, a two-dimensional sheet is deformed within a rectangular box (Fig. 2b). Transport direction is held strictly unidirectional toward the foreland. Deformation takes place within an oblique deformation zone which makes an angle α with the transport direction. This oblique deformation zone can be viewed as a segment of an arcuate fold–thrust belt (Fig. 2a). Deformation is imposed within this zone by advancing a rigid hinterland indenter. For simplicity, deformation is assumed to be homogeneously consumed within the entire north–south length of the deformation zone, and without any slip on the limits between foreland, deformation zone and rigid hinterland indenter. North–south oriented marker lines thus remain perfectly straight and do not rotate. In other words, no material is allowed to be squeezed out on the right- or left-hand side of the modeled arc segment shown in Fig. 2(b). For comparisons with the starting conditions, the left-hand side of Fig. 2(b) shows an undeformed row with grid numbers for a rapid identification of corresponding positions in the deformed grid of the arc segment. Given these boundary conditions, finite strain within the modeled deformation zone is homogeneous and can be calculated. Geometrically, finite strain can easily be understood as the superposition of a pure shear deformation followed by a simple shear deformation. The pure shear component is required to shorten any north–south line to its deformed length (W) as imposed by the advance (D) of the indenter. The 'pure shear' shortening in transport direction (ps) is calculated as the length change (D) over the initial

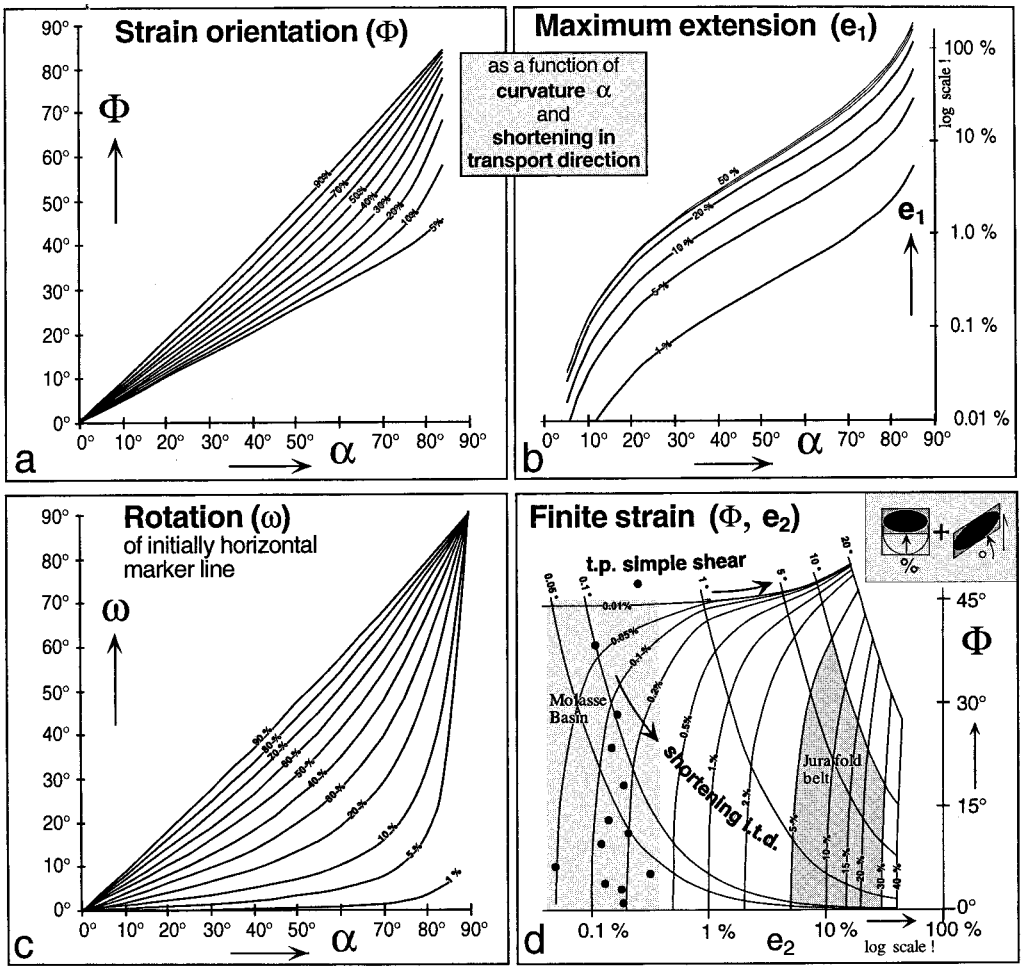

Fig. 3. Strain parameters resulting from deformation in an oblique arc segment shown in Fig. 2(b): (a) Finite strain orientation (Φ) with respect to transport direction vs the obliquity of the deformation zone (α) as a function of variable amounts of 'pure shear' shortening in transport direction (indicated in % along the curves). (b) Maximum extension (e_1, finite strain) in % on a logarithmic scale vs the obliquity of the deformation zone (α) as a function of variable amounts of 'pure shear' shortening in transport direction (indicated in % along the curves). (c) Rotation (ω) of an initially transport perpendicular marker line vs the obliquity of the deformation zone (α) as a function of variable amounts of 'pure shear' shortening in transport direction (indicated in % along the curves). (d) The effects of the superposition of variable amounts of 'pure shear' in transport direction (expressed as % shortening) followed by transport parallel simple shear (expressed as the angle of simple shear) are illustrated in terms of resulting finite strain orientation (Φ) and maximum shortening (e_2) expressed as % on a logarithmic scale. Calcite twinning strain determinations from the Swiss Molasse basin are reported as black dots within a grey shaded box at the left-hand side of the graph, a second box at the right-hand side illustrates the estimated strain field for the Jura fold–thrust belt (compare Fig. 4).

length ($W + D$):

$$\mathrm{ps} = D/(W + D) \tag{1}$$

A component of 'transport parallel' simple shear (ss) is required to twist this shortened material into the oblique deformation zone in order to avoid any misfit between the deformed zone, its foreland and the rigid hinterland indenter, respectively. The simple shear component is calculated as:

$$\mathrm{ss} = \mathrm{ps} * \tan(\alpha). \tag{2}$$

Rotations (ω) of initially horizontal passive marker lines (perpendicular to the transport direction) result from the simple shear component of deformation and are calculated as:

$$\omega = \arctan(\mathrm{ps} * \tan(\alpha)). \tag{3}$$

Rotations in general are dependent on the initial orientation of a marker line and decrease to zero for marker lines oriented parallel to the transport direction.

Some of the most striking results of these considerations are shown graphically in Fig. 3. The orientation of finite strain axes orientation (Φ) has been calculated as a function of the amount of shortening in transport direction (ps) and for variable curvatures (α) in Fig. 3(a). Note that even very weak shortening in transport direction within an oblique deformation zone leads to considerable deviations of the finite strain axes from an 'expected' orientation perpendicular to the imposed

transport direction. Maximum horizontal extensions (e_1) are calculated as a function of the curvature and shortening in transport direction in Fig. 3(b). Extensions increase exponentially with curvature and shortening in transport direction. However, Fig. 3(b) clearly illustrates the difficulty associated with the identification of any obliquity between transport direction and finite strains as seen in a fold–thrust belt. Consider an oblique deformation zone with an angle α of 45° and a shortening of 30% in transport direction. The resulting arc-parallel stretching of around 5% only may easily go unnoticed! Passive rotations (ω) of an initially horizontal marker line have been calculated as a function of the amount of shortening in transport direction (ps) and for variable curvatures (α) in Fig. 3(c). This figure shows that passive rotations are a significant component of strain within an oblique deformation zone (Fig. 2b); passive rotations are in all cases less than the obliquity of the deformation zone (α) and less than the long axis orientation of the finite strain ellipse produced within this deformation zone (compare Fig. 3c with Fig. 3a).

More general models of oblique deformation zones can be set up by varying the width W along strike, by varying both outer and inner curvature of the belt, i.e. angles α and β in Fig. 2(a), by varying the total imposed displacement D along strike and so on (Hindle, 1996). In all such models, deformation within the deformation zone can be viewed as the superposition of variable amounts of 'pure shear in transport direction' and 'transport parallel simple shear'. The relative importance of these two deformations determines the deviation of the principal finite strain axis orientation (Φ) from the transport direction. The general case of superimposed transport parallel simple shear on pure shear shortening in transport direction is shown in Fig. 3(d) which demonstrates that large deviations of up to and more than 45° between the maximum finite shortening direction (e_2) and the transport direction are obtained even in very weakly deformed transpressive zones.

A counterintuitive conclusion of these models is that very weak simple shearing deformations within an arc (and its hinterland) are capable of producing strong deviations between strain axes orientations and transport direction (non-coaxial deformations). Furthermore, the extremely simple model set-up of Fig. 2(b) demonstrates that deformations within an oblique deformation zone with parallel foreland and hinterland borders ($\alpha = \beta$), will provoke rotations (ω) in passive marker lines with progressively increasing advance of the hinterland indenter by the distance D.

Some key points regarding strains within an arc formed by the 'primary arc' model with uniform displacement direction are summarized as follows. Compressional deformation across the arc is accompanied by longitudinal extension in a direction close, but not parallel to the structural grain of the arc's 'limbs'. The amount of this extension is strongly dependent on the intensity of simple shear deformation and increases non-linearly with increasing angle of the 'limbs' of the arc (α). The direction of maximum extension is oblique to both the overall 'limb' angle and the transport direction (Fig. 2b). The fact that an arc-parallel line of 'no finite longitudinal strain' exists in this model has often been misinterpreted in the sense that no longitudinal extensions existed at all (Ries and Shackleton, 1976, fig. 2a; Ferrill, 1991, fig. 18). This line, however, is merely one of two symmetric lines of no finite extension within the general strain ellipse produced by transpression (our Fig. 2b). Rotations are a direct consequence of the simple shear component and increase with the increasing angle of the 'limbs' of the arc and with increasing shortening in transport direction.

Marshak (1988) proposed a modified, loosened definition of Carey's 'orocline', as 'a bend in which the strike of segments of the bend *does change* during and/or subsequent to the formation of the orogen' (op. cit. p. 74). This type of arc is opposed to the 'non-rotational' bend, 'in which the strike of segments of the bend *does not change* during the formation of the orogen' (Marshak, 1988, p. 74). Such a distinction of arcs is problematic for several reasons: The primary arc model sketched in Fig. 2(b) demonstrates that progressive compressional deformation within an oblique deformation zone necessarily leads to rotations of passive marker lines and to a progressive rotation of the structural grain in the oblique deformation zone. The term 'strike' used by Marshak with regard to rotations during arc formation is not clearly defined and would apply only to the boundaries between a rigid hinterland indenter and a deformation zone (β) or the limit between the latter and a rigid foreland (α, compare Fig. 2a), but the term 'strike' does not apply to the structural grain within the deformation zone itself. We pretend that there is no two-dimensional or three-dimensional arc formation model which is capable of producing a bend in a compression belt without involving rotations of *some* passive marker lines seen in map view of this belt. Nevertheless, a non-rotational arc fitting the above quoted definition of Marshak (1988) does exist: in our classification, it would be a 'primary arc' with divergent transport directions (as in the 'Piedmont glacier' type). Transport directions would have to be strictly perpendicular to the imposed, preexisting arc shape ('strike of the arc')—passive marker lines in general would be rotated, but not the 'strike' of the arc. Our own classification scheme of arcs suffers from a similar problem. Using the 'displacement vector field' rather than strains, rotations or shape as the main criterion to distinguish different

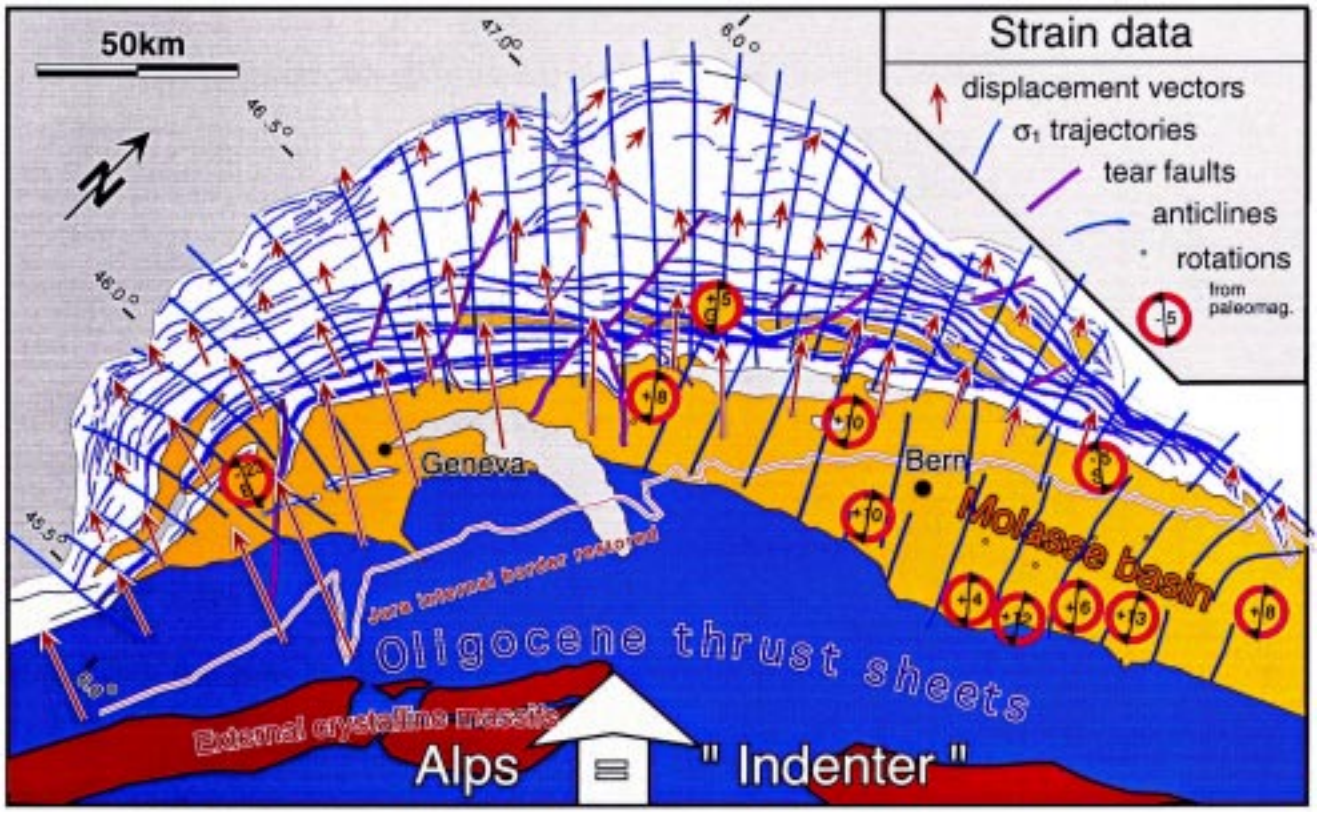

Fig. 4. Tectonic overview of the Jura arc in front of the northwestern Alps with compiled strain data. The arcuate shape of the Jura is materialized by the trend of major anticlines (Heim, 1921). Strain trajectories (in blue) have been computed from a large data set of 180 stations where populations of minor faults have been used to calculate paleo-stress tensors by inversion methods (Homberg, 1996). Strain trajectories within the Molasse basin are based on striated and indented pebbles (Schrader, 1988) and twinned calcite cements (Hindle, 1996). Displacement vectors (red, to scale) are based on balanced cross-sections augmented by 'block mosaic' restorations in map view (Philippe et al., 1996). A thin red line marks the approximate restored position of the inner boundary of the Jura arc. Rotations have been paleomagnetically determined by Kempf et al. (1998) with three additional sites from Gehring et al. (1991), Burbank et al. (1992) and Schlunegger et al. (1996), marked G, B and S, respectively. Oligocene data have been corrected systematically by -10° according to a paleo-pole from Besse and Courtillot (1991).

types of arcs, we rely on the one parameter which is the most difficult to obtain in a natural deformation belt. These difficulties and possible ways to resolve them are discussed in the following section where the Jura arc of the external Alps is discussed.

4. The Jura arc

4.1. Tectonic overview

The structural grain of the Jura arc in the northwest foreland of the Alps swings a full 90° from a north–south direction at the southwest end to an east–west direction at the northeast end (Fig. 4). This latest and most external fold–thrust belt of the Alps developed after the Middle Miocene (Serravallian) on the external side of the Molasse foredeep (Laubscher, 1992; Burkhard and Sommaruga, 1998). Mesozoic platform carbonates (up to 2.5 km) as well as an Oligo-Miocene clastic Molasse wedge (0–4 km) are involved in folding and thrusting above a major basal décollement within Triassic evaporites (Buxtorf, 1916; Jordan, 1994; Sommaruga, 1997). The paleogeography of the Triassic 'Muschelkalk' and 'Keuper' series is largely responsible for the arcuate shape of the Jura fold–thrust belt (Debrand-Passard et al., 1984; Philippe, 1994). The external border of the Jura arc coincides with the salt/gypsum pinchout and the arc mimics directly the original shape of the Triassic basin border. The western and eastern limbs of the Jura arc owe their asymmetry to paleogeography. In addition to lateral variations in the basal décollement level, a lateral increase in total thickness of the folded Mesozoic cover explains a striking westward increase in fold amplitude and wavelength. While the outer curvature of the Jura arc can largely be interpreted in terms of paleogeographic prestructuration, the inner curvature, i.e. the rather abrupt change between virtually undeformed Molasse basin and strongly folded and thrusted Jura, still remains a matter of debate. It could be induced by the late variscan structural grain within

the pre-Triassic basement (Philippe, 1995). Reflection seismic surveys across this boundary at the eastern termination of the Jura show some weak normal fault offsets in the Triassic series above the Permo-Carboniferous grabens and below the basal décollement (Diebold et al., 1991). Such irregularities within the Triassic basal décollement horizon are thought to have triggered major thrust fault splays breaking through to the surface across the entire Mesozoic cover sequence (Laubscher, 1986). In terms of critical taper geometry (Chapple, 1978; Dahlen, 1990) the internal border of the Jura arc may simply be regarded as the line behind which the taper angle of the combined thickness of Mesozoic and Neogene sediments was sufficient for thrust translation whereas north of this line, some internal deformation, thickening and increase of topographic slope was a requirement for further thrust propagation to the northwest. The Jura fold–thrust belt is located above the present day flexural bulge region in the alpine foreland (Karner and Watts, 1983; Burkhard and Sommaruga, 1998), an area where the cover thickness is at a minimum.

A large amount of strain data has been collected over the last decades within the curved Jura fold–thrust belt. Different categories of strain measurements can be distinguished; they are discussed below.

4.2. Strain measurements and their relevance to arc formation

4.2.1. Two-dimensional cross-section balancing

The best large-scale strain estimates are provided by balanced cross-sections, available at various degrees of sophistication for all parts of the Jura. Bulk shortening perpendicular to the fold trends ranges from more than 35 km (in west–east direction) in western parts to some 25 km (in northwest–southeast direction) in central parts (Mugnier et al., 1990; Philippe, 1995). Towards the east, bulk shortening decreases regularly to zero (Laubscher, 1965; Bitterli, 1988; Burkhard, 1990). Despite their accuracy, estimated at better than 20%, cross-section balancing results are incomplete measures of strain. Transport directions are an input—assumed to be known—and not an output of cross-section balancing techniques. The postulate of no material moving in or out of section sideways obviously limits their applicability within oblique deformation zones of wrench folding. In terms of arc formation models and attempts at their discrimination, three-dimensional strains or at least estimates of the arc parallel extensions are required in addition to the shortenings obtained from two-dimensional section balancing.

4.2.2. Strain trajectories

The Jura fold–thrust belt was deformed under very little cover, mostly less than 1 km, at temperatures well below 100°C. Accordingly, outcrop and hand-specimen scale deformation features are limited to joints, veins, faults and tectonic stylolites. Cleavage development is restricted to the proximity of larger faults and shear zones within marl and shale horizons. The systematic mapping of meso-scale strain-axes orientations includes tectonic 'horizontal' stylolite peaks (Plessmann, 1972) interpreted as indicators of the local maximum horizontal shortening direction. Small-scale striated faults with displacements on the order of a few mm to dm are a widespread phenomenon, seen in virtually any fresh outcrop of limestones be it folded or subtabular. Most minor fault surfaces in Jura limestones carry slickenfibers, slickolites or some asymmetric wear-features on slickensides which enable an easy identification of both displacement direction and shear sense. The systematic measurement of many small-scale faults and their inversion at any given site permits the determination of paleo-stress (or strain-) axes directions (Angelier, 1994). The most complete paleo-stress data set to date has been acquired by Homberg (1996). This data set includes 180 sites, often with up to four successive deformation phases distinguished. The latest and most important Mio-Pliocene folding phase data have been used to construct a 'strain trajectory-map' (Fig. 4, blue lines) according to an interpolation- and smoothing-procedure which considers the spatial distribution of sites as well as the data quality at each site (Dick, 1998, unpublished; using software provided by Lee and Angelier, 1994). The deformation style in the Jura alternates between a dominant thrusting regime with a subordinate strike-slip component. The former is expressed in conjugate small-scale thrust faults and bedding parallel slip planes associated with folds while the latter is materialized in the form of conjugate sets of strike-slip faults at a high angle to bedding. Both thrusts and strike-slip faults were active simultaneously and no relative chronology can be established between the two regimes (Laubscher, 1972; Tschanz and Sommaruga, 1993; Homberg et al., 1997).

Micro-scale strain-determinations from twinning in calcite (Tschanz, 1990) reveal shortening directions which are mostly at high angles to the map scale fold axes; local obliquities have been interpreted in terms of wrench folding (Tschanz and Sommaruga, 1993). These techniques have also been used to reconstruct the alpine paleo-stress field in front of the Jura fold–thrust belt (Bergerat, 1987; Lacombe et al., 1993). In order to complete the regional scale strain data set we determined micro-strains within the flat-lying layers of the Molasse basin adjacent to and behind the Jura arc. Microscopic investigation of a competent member of lower Miocene marine Molasse sandstones revealed the ubiquitous presence of deformation twinning in

calcite cements and bioclasts. Calcite grains larger than about 10 μm are frequently twinned and permit the determination of strain orientations and magnitudes. We used the Groshong (1972) technique to determine strains within the apparently un-deformed Molasse rocks (Hindle, 1996). Our study fills an important gap in the central, hinterland portion of the Jura arc. Twin strain data indicate minute strains, between 0.01 and 1% shortening and extension, respectively. The strain regime varies between thrust and strike slip. Detailed data tables are found on an internet site (Burkhard, 1999).

At the southern border of the Molasse basin, conglomerates show macroscopic evidence for horizontal tectonic compression in the form of striations, slickolites and stylolites on 'pitted' carbonate pebbles (Schrader, 1988). A regional scale survey of these features has enabled Schrader (1988) to construct a strain trajectory map for the southern rim of the Molasse basin (included in our Fig. 4). Based on the symmetry of strain features on conglomerates, Schrader was also able to characterize the form of the strain ellipsoid, which varies between oblate (pure compression) and plane strain, often in a strike-slip regime.

The strain trajectory map shown in Fig. 4 describes a strongly divergent, radial pattern with northeast–north directed compression at the eastern end of the Jura and west-directed compression behind the western termination of the arc. This gross pattern confirms the large-scale structural trend of the Jura fold–thrust belt as depicted by a tectonic map (Heim, 1921, tafel XX). Local irregularities in the strain trajectory map and detailed relationships between tear faults, faults and 'background strain' axes directions are discussed by Homberg et al. (1997) in terms of stress-deviations in the vicinity of major tear faults. So far, however, no attempts at integrating the strain-trajectories into balancing considerations, be it two-dimensional or three-dimensional have been made in the case of the Jura arc.

4.2.3. Three-dimensional restorations ⇒ displacement vector field

Three-dimensional balancing work in the Jura was pioneered by Laubscher (1961, 1965) who developed what he called the 'block mosaic' restoration technique. The Basel school applied it to eastern parts of the Jura fold–thrust belt in ever increasing detail (e.g. Bitterli, 1988). In essence, the 'block mosaic' technique is based on a series of balanced two-dimensional sections, made mutually compatible with each other by trial and error. Restored bedding surfaces or 'three-dimensional blocks' are obtained by filling spaces in between balanced sections. In this technique neither the true surface of marker horizons nor their capacity to 'unfold' without bed internal stretching (Lisle, 1992) is verified. Similarly, in the 'pseudo-three-dimensional approach' of Wilkerson et al. (1991, fig. 1) oblique folds are produced and balanced without any consideration of true three-dimensional bed-internal stretches required to allow for the differential displacements in the first place. Gratier and Guillier (1993) have developed a more objective 'UNFOLD'-method of smoothing out entire contour maps of folded marker beds. Folds in this technique are still treated as 'folds in a sheet of paper', however, no stretches are allowed within the sheet itself. With this premise, folds are always restored in a direction perpendicular to their fold axis. Smooth folds in a 'sheet of paper' cannot form in a direction oblique to the transport direction (e.g. in a model such as shown in Fig. 2b). Wrench folds require the development of tear faults or some other kind of intrabed strain. Both Laubscher's and Gratier's approaches at three-dimensional restoration stand and fall with the quality of the initially drawn cross-sections and contour-maps. Applied to faulted and thrusted rocks, the most important uncertainties do not reside with the smoothing out of individual folds, but with ill-defined fault offsets between different folds and along tear faults, and from unknown intrabed stretches. When it comes to reassemble unfolded (restored) blocks in a possible prefolding configuration, Laubscher's and Gratier's approaches are identical and meet with the same difficulties. Thrust fault offsets are constrained from section balancing whereas no direct way exists to determine offsets along tear faults. In assembling unfolded pieces of a flattened structure contour map, gaps and overlaps indicate the quality of the 'block mosaic' restoration. Reducing these incompatibilities is a time consuming trial-and-error process which may include reassessment of initially drawn contour maps—and possibly the search for previously undiscovered tear faults. Automated procedures to minimize such incompatibilities have been proposed by Cobbold (1979) but are rarely applied in regional studies (Gratier et al., 1989). The comparison between a completely restored and reassembled 'block mosaic' and the present day deformed state (structure contour map) permits the determination of a displacement vector field as well as the calculation of inferred regional strains in planform.

Large-scale tear faults affect the Jura arc at regular intervals of some tens of kilometers. North–south-trending sinistral faults are more important than conjugate dextral ones (major tear faults are shown in purple in Fig. 4). Some of the north–south-trending faults inherited their orientation from Oligocene faults formed during development of the Rhine–Bresse graben system (Illies, 1974), while others were demonstrably formed only during Late Miocene Jura folding and thrusting (Homberg et al., 1997). Tear faults clearly accommodate some arc-parallel extension (Heim, 1915)

which is difficult to quantify because of the lack of suitable passive markers. Folds clearly developed independently on either side of tear faults, simultaneously with tearing, and cannot be used as markers. Block mosaic restorations, backward from the undeformed foreland into the increasingly deformed hinterland, is the only way to determine the map-scale strains associated with these faults in particular and the entire displacement vector field on the scale of the arc in general. Our own restorations in the central Jura (Hindle, 1996) as well as those of Philippe (1995) in the western Jura, indicate that fold axes parallel extensions do not exceed a few percent.

The most complete three-dimensional block mosaic restoration of the entire Jura so far has been constructed by Philippe et al. (1996). The displacement vector field derived from this restoration is shown in Fig. 4 (red arrows, drawn to scale). Despite some divergence in this displacement vector field, there exists a marked difference between displacement vectors and the significantly more divergent strain trajectories (in blue). Discrepancies are largest in the western limb of the Jura arc (30° and more). Not surprisingly, coaxial deformations prevail in the central portion of the Jura and discrepancies increase again eastward. Due to small total displacements at the right-hand side of the arc, however, discrepancies are not so obvious. Given the limitations in the three-dimensional block mosaic restoration procedure discussed above, the true displacement vector field for the Jura arc can be expected to be less divergent than shown in Fig. 4. In the restoration used by Philippe et al. (1996) only the largest tear faults (purple in Fig. 4) have been included as free boundaries in the re-assemblage of internally non-stretched flattened blocks. Intrabed wrenching deformations do occur within those blocks, however, as testified by meso-scale fault analyses which show often a component of strike-slip deformation regime (Homberg, 1996).

4.2.4. Rotations about vertical axes

Based on map-scale restorations, Laubscher (1961) proposed a rotation model to account for the westward increase of shortening seen in the Jura fold–thrust belt, estimated at some 8° clockwise for the Molasse basin behind the eastern part of the Jura (compare the thin red line behind the internal Jura in Fig. 4). Similarly, the strong westward decreasing lengths of sub-parallel displacement vectors behind the western limb of the Jura arc (Fig. 4; data from Philippe et al., 1996) implies a substantial anticlockwise rotation of material in a sinistral wrenching regime. These expected rotations are still small, however, in comparison with the strong curvature of the limbs of the arc which swing a full 90° angle. Given the lack of suitable passive marker lines, rotations about vertical axes are notoriously difficult to measure directly. Some constraints on rotations are provided by paleomagnetic data. While older studies in Middle Jurassic iron oolithes of the Jura fold belt (Eldredge et al., 1985; Gehring et al., 1991) detected only very small and barely significant clockwise rotations of less than 10°, two recent studies in Oligo-Miocene Molasse sandstones from the hinterland of the Jura have identified small but systematic clockwise deviations of paleo-poles from present day geographic north, on the order of 5–25° (Schlunegger et al., 1996; Kempf et al., 1998). There are only two published sites from behind the western half of the Jura (Burbank et al., 1992). The combined result of the Findreuse and Fornant sections shows a small anticlockwise rotation of ca. 13° from the present day geographic north (although this deviation was not considered as significant by the authors). The tectonic interpretation of the paleomagnetically determined declinations for Oligocene Molasse sandstones is somewhat hampered by the fact that there are no directly comparable sites available for the undeformed foreland of the Jura. The maximum difference between paleo-pole declinations east and west of the symmetry axis of the Jura arc is on the order of 30–35° for rocks of the same Oligocene age. According to Besse and Courtillot (1991), the European paleo-pole position for Oligo-Miocene times was located some 10° to the 'east' of the present day geographic pole. Accordingly, tectonic rotations shown in Fig. 4 have been systematically corrected by −10° with respect to the published declinations (see also discussion in Kempf et al., 1998).

A fundamental question in rotation studies regards the strain partitioning and deformation mechanisms leading to the rotation of 'passive' marker lines. Perfectly homogeneous deformation within an oblique deformation zone, such as modeled in Fig. 2, can be opposed to perfectly rigid blocks, rotated in between discrete faults. In the latter case, block rotations are strongly dependent on the organization and hierarchy of faults in a fault network. Analog experiments of dextral simple shear (Schreurs, 1994) provide some interesting insights into the relationships between distributed background strain and localized faults. In the simple shear model of Schreurs (1994, fig. 2a and b), distributed 'homogeneous' deformation is dominant in early stages (γ up to 0.17) leading to rotations of transport perpendicular marker lines up to 10°. Transport parallel lines have not rotated at all. In later stages ($\gamma = 0.17$–0.39), rotations increase locally to about 30° clockwise between synthetic 'cross faults', more than the overall total 21° rotation imposed by dextral simple shear! However, transport parallel marker lines are significantly less rotated, indicating that internal 'distributed' strains are an important component. The question arises if and how paleomagnetically deter-

mined paleo-pole directions are affected by weak internal deformations. Assuming that such internal deformations of up to 10–20% stretching/shortening are not sufficient to have any effect on the minute magnetic particles and their distribution in a rock, the paleomagnetic method provides a very powerful tool to determine 'rigid block' rotations. The size of such rotated 'blocks' is certainly larger than the rock sample, but probably smaller than the average mapped distance between major faults in an area. Large-scale tectonic interpretations are limited by our sketchy knowledge about the organization of intermediate size faults, fault networks and their rotation effects on 'blocks' in between them.

Significant improvements of three-dimensional balancing could probably be obtained by the integration of micro- and meso-scale observations into large-scale three-dimensional restorations. Fault patterns observed in the outcrop have been used so far only for the construction of paleo-stress directions; the same data sets, augmented with displacement–lengths–frequency observations could provide very useful estimates of fault-related strain magnitudes (Scholz and Cowie, 1990; Cowie and Scholz, 1992). Similarly, paleomagnetically determined 'block' rotations provide an additional constraint on fault related intra-bed strains on a larger scale.

5. Conclusions

1. A straight-forward genetic classification scheme of arcs into three end-member models is proposed. Key parameters are the displacement vector fields and the resulting finite strain patterns. The identification of mechanisms which lead to the formation of arcuate mountain belts relies on the recognition and mapping of subtle large-scale strain components such as bulk arc-parallel extensions and rotations about vertical axes. Neither of these quantities are obtained from the routinely applied two-dimensional balancing of cross-sections, which require an a priori knowledge of transport direction.
2. The intuitive interpretation of arcuate fold belts as 'virgations du premier genre' (Argand, 1924), with fanning transport directions as seen in 'Piedmont glaciers' should not be accepted in the absence of positive arguments such as large arc-parallel extensions in the outer, frontal portions of the arc. Rotations and arc-parallel extensions in the limbs of arcs, generally used as arguments in favor of either 'oroclinal bending' or 'divergent spreading' do also result from the superposition of variable amounts of pure and simple shear in the transport direction even in a strictly parallel displacement vector field of 'primary arcs'.
3. Strain determinations on all scales are available for the late Miocene Jura arc which shows a marked 90° change in structural grain as well as a radial pattern in mesoscopic strain trajectories. Deformation type varies between pure shear compression (thrusts and folds) and strike-slip faults on all scales. Strain trajectories show a strongly fanning pattern with a 90° divergence (Homberg, 1996).
4. Three-dimensional restorations of the Jura arc (Philippe et al., 1996) are based on section balancing data, augmented with 'block mosaic' restorations. The resulting displacement vectors diverge by about 40°, markedly less than strain trajectories. Non-coaxiality between displacement vectors and strain axes indicates significant wrenching deformations in both limbs of the Jura arc.
5. Bulk arc-parallel stretches are difficult to determine; estimates based on three-dimensional restorations reveal only minor amounts of less than 10%. Integration of small-scale strain features such as 'distributed' tear faults in three-dimensional restorations would probably increase arc parallel stretches and at the same time decrease divergence in the displacement vector field.
6. Rotations about vertical axes are predicted by three-dimensional restorations and constrained by some paleomagnetic measurement sites. Rotations in the Jura arc and its hinterland are barely detectable and range from 0 to 25°, much less than the 90° change in strike around the arc. This discrepancy is a strong argument against pure 'oroclinal bending' and 'Piedmont glacier' type spreading. The small observed rotations are best explained by passive rotations in a wrenching regime. The size of individual 'rigid' rotated blocks remains undetermined.
7. We conclude that the Jura formed as a 'primary arc' with a dominant northwestward displacement direction and some spreading of material sideways, i.e. a component of 'Piedmont glacier' type. Transport parallel simple shear combined with variably consumed pure shear in the transport direction provides the most satisfying explanation to the strains observed in and around the Jura arc at all scales.
8. Arc formation studies will greatly benefit from future developments of true three-dimensional balancing techniques and the integration of micro- and meso-scale strain determinations into regional scale three-dimensional restorations. This is the only way to obtain the single most important item in arc classification schemes: the total displacement vector field.

Acknowledgements

This study was supported by the Swiss National Science Foundation Grants No. 20-43055.95 and 20-50535.97; it represents part of the PhD thesis of D.H. We should like to express thanks to Ph. J. Keane at the Science and Technology Library, University of Tasmania, for promptly sending us a copy of Carey's paper; F. Schlunegger, O. Kempf and P. Strunck for preprints of papers with paleomagnetic data; Y. Philippe and C. Homberg for unpublished manuscripts of their theses. Discussions with A. Becker, O. Besson, P. Dick (thanks for producing the strain trajectory map), D. Ferrill, J. P. Gratier, R. Groshong, C. Homberg, G. Schönborn have helped to shape our ideas about arc formation. S. Marshak and J. P. Evans are thanked for helpful reviews.

Appendix

Two annexes of data available on the internet at the following address: http://www-geol.unine.ch/Structural/DHdata.html

Annex 1: Data table with twinning strain data from the Swiss Molasse basin.

Annex 2: Stereograms with twinning strain data from the Swiss Molasse basin.

References

Angelier, J., 1994. Fault slip analysis and paleostress reconstruction. In: Hancock, P.L (Ed.), Continental Deformation. Pergamon Press, Oxford, pp. 53–100.

Argand, E., 1924. La tectonique de l'Asie. In: 13th International Geological Congress Conf. Proceedings, Brussels, p. 171.

Bergerat, F., 1987. Paléo-champs de contrainte tertiaires dans la plate-forme européenne au front de l'orogène alpin. Bulletin de la Société géologique de France 8, 611–620.

Besse, J., Courtillot, V., 1991. Revised and synthetic apparent polar wander path of the African, Eurasian, North American and Indian plates, and true polar wander since 200 Ma. Journal of Geophysical Research 96, 4029–4050.

Bitterli, T., 1988. Die dreidimensionale Massenbilanz—ein wichtiges Hilfsmittel zum Verständnis der regionalen Kinematik (Schuppenzone von Reigoldswil, Faltenjura). Eclogae geologicae Helvetiae 81, 415–431.

Burbank, D.W., Engesser, B., Matter, A., Weidmann, M., 1992. Magnetostratigraphic chronology, mammalian faunas, and stratigraphic evolution of the Lower Freshwater Molasse, Haute-Savoie, France. Eclogae geologicae Helvetiae 85, 399–431.

Burkhard, M., 1990. Aspects of the large scale Miocene deformation in the most external part of the Swiss Alps (Subalpine Molasse to Jura fold belt). Eclogae geologicae Helvetiae 83, 559–583.

Burkhard, M., 1999. http://www-geol.unine.ch/Structural/DHdata.html, Data tables of calcite thin strain data.

Burkhard, M., Sommaruga, A., 1998. Evolution of the western Swiss Molasse basin: structural relations with the Alps and the Jura belt. In: Mascle, A, Puigdefàbregas, C, Luterbacher, H.P, Fernàndez, M (Eds.), Cenozoic Foreland Basins of Western Europe, vol. 134. Geological Society Special Publications, London, pp. 279–298.

Buxtorf, A., 1916. Prognosen und Befunde beim Hauensteinbasis- und Grencherberg-tunnel und die Bedeutung der letzeren für die Geologie des Juragebirges. Verhandlungen der Naturforschenden Gesellschaft in Basel 27, 184–205.

Carey, S., 1955. The orocline concept in geotectonics. Proceedings Royal Society Tasmania 89, 255–288.

Chapple, W.M., 1978. Mechanics of thin-skinned fold-and-thrust belts. Geological Society of America Bulletin 89, 1189–1198.

Cobbold, P.R., 1979. Removal of finite deformation using strain trajectories. Journal of Structural Geology 1, 67–72.

Cowie, P.A., Scholz, C.H., 1992. Displacement–length scaling relationship for faults: data synthesis and discussion. Journal of Structural Geology 14, 1149–1156.

Dahlen, F.A., 1990. Critical taper model of fold-and-thrust belts and accretionary wedges. Annual Review of Earth and Planetary Sciences 18, 55–99.

Debrand-Passard, S., Courbouleix, S., Lienhardt, M.-J., 1984. Synthèse géologique du Sud-Est de la France. Stratigraphie et Paléogéographie, Orléans.

Diebold, P., Naef, H., Amman, M., 1991. Zur Tektonik der Zentralen Nordschweiz. Nagra, Baden.

Eldredge, S., Bachtadse, V., Van der Voo, R., 1985. Paleomagnetism and the orocline hypothesis. Tectonophysics 119, 153–179.

Ferrill, D.A., 1991. Curvature development and limestone deformation in the northern subalpine chain (Haute Savoie, France). Unpublished PhD thesis, University of Alabama.

Ferrill, D.A., Groshong, R.H.J., 1993. Kinematic model for the curvature of the northern Subalpine Chain, France. Journal of Structural Geology 15, 523–541.

Gehring, A.U., Keller, P., Heller, F., 1991. Paleomagnetism and tectonicas of the Jura arcuate mountain belt in France and Switzerland. Tectonophysics 186, 269–278.

Gratier, P., Guillier, B., 1993. Compatibility constraints on folded and faulted strata and calculation of total displacement using computational restoration (UNFOLD program). Journal of Structural Geology 15, 391–402.

Gratier, J.P., Ménard, G., Arpin, R., 1989. Strain–displacement compatibility and restoration of the Chaînes Subalpines of the western Alps. Alpine tectonics (ed. Coward, M., et al.) Special Publication of the Geological Society of London, 45, 65–81.

Groshong, R.H., 1972. Strain calculated from twinning in calcite. Geological Society of America Bulletin 82, 2025–2038.

Heim, A., 1915. Die horizontalen Transversalverschiebungen im Juragebirge. Geol. Nachlese Nr. 22. Verhandlungen Naturforschende Gesellschaft Zürich 60, 597–610.

Heim, A., 1921. Geologie der Schweiz. Band I Molasseland und Juragebirge. Tauchniz, Leipzig.

Hindle, D.A., 1996. Quantifying stresses and strains from the Jura Arc, and their usefulness in choosing a deformation model for the region. Unpublished PhD thesis, Neuchâtel University.

Homberg, C., 1996. Analyse des déformations cassantes dans le Jura et modélisation numérique des perturbations des contraintes tectoniques autour d'accidents majeurs. Unpublished PhD thesis, Université de Paris VI, France.

Homberg, C., Hu, J.C., Angelier, J., Bergerat, F., Lacombe, O., 1997. Characterization of stress perturbations near major fault zones: insights from 2-D distinct element numerical modelling and field studies (Jura mountains). Journal of Structural Geology 19, 703–718.

Illies, J.H., 1974. Taphrogenesis and plate tectonics. In: Illies, J.H, Fuchs, K (Eds.), Approaches to Taphrogenesis, Geodyn., Sci. Rep, 8. Schweizerbart'sche, Stuttgart, pp. 433–460.

Isacks, B.L., 1988. Uplift of the central Andean plateau and bending

of the Bolivian orocline. Journal of Geophysical Research 93, 3211–3231.

Jordan, P., 1994. Evaporite als Abscherhorizonte. Eine gefügekundlich-strukturgeologische Untersuchung am Beispiel der Nordschweizer Trias. Matériaux Carte Géologique Suisse [n.s.] 164, 79.

Karner, G.D., Watts, A.B., 1983. Gravity anomalies and flexure of the lithosphere at mountains ranges. Journal of Geophysical Research 88, 10449–10477.

Kempf, O., Schlunegger, F., Strunck, P., Matter, A., 1998. Paleomagnetic evidence for late Miocene rotation of the Swiss Alps: results from the north Alpine foreland basin. Terra Nova 10, 6–10.

Lacombe, O., Angelier, J., Byrne, D., Dupin, J.M., 1993. Eocene–Oligocene tectonics and kinematics of the Rhine–Saone continental transform zone. Tectonics 12, 874–888.

Laubscher, H.P., 1961. Die Fernschubhypothese der Jurafaltung. Eclogae geologicae Helvetiae 54, 221–280.

Laubscher, H.P., 1965. Ein kinematisches Modell der Jurafaltung. Eclogae geologicae Helvetiae 58, 232–318.

Laubscher, H.P., 1972. Some overall aspects of Jura dynamics. American Journal of Science 272, 293–304.

Laubscher, H.P., 1986. The eastern Jura: Relations between thin-skinned and basement tectonics, local and regional. Geologische Rundschau 75, 535–553.

Laubscher, H.P., 1992. Jura kinematics and the Molasse basin. Eclogae geologicae Helvetiae 85, 653–676.

Lee, J.C., Angelier, A., 1994. Paleostress trajectories maps based on the results of local determinations: the 'lissage' program. Computer and Geosciences 20, 161–191.

Lisle, R.J., 1992. Constant bed-length folding: three dimensional geometrical implications. Journal of Structural Geology 14, 245–252.

Lowrie, W., Hirt, A.M., 1986. Paleomagnetism in arcuate mountain belts. In: The Origin of Arcs. Developments in Geotectonics, vol. 21. Elsevier, Amsterdam, pp. 141–158.

Marshak, S., 1988. Kinematics of orocline and arc formation in thin-skinned orogens. Tectonics 7, 73–86.

Marshak, S., Wilkerson, M.S., Hsui, A.T., 1992. Generation of curved fold-thrust belts: Insight from simple physical and analytical models. In: McClay, K (Ed.), Thrust Tectonics. Chapman & Hall, London, pp. 83–92.

Merle, O., 1989. Strain models within spreading nappes. Tectonophysics 165, 57–71.

Mugnier, J.L., Guellec, S., Ménard, G., Roure, F., Tardy, M., Vialon, P., 1990. A crustal scale balanced cross-section through the external Alps deduced from the ECORS profile. In: Roure, F, Heitzmann, P, Polino, R (Eds.), Deep Structure of the Alps, vol. 1. Mém. Soc. géol. suisse, Zürich, pp. 203–216.

Philippe, Y., 1994. Transfer zone in the Southern Jura Thrust Belt (eastern France): Geometry, development and comparison with analogue modelling experiments. In: Mascle, A. (Ed.), Hydrocarbon and Petroleum Geology of France (special issue). European Association of Petroleum Geology Special Publication 4, 327–346.

Philippe, Y., 1995. Rampes latérales et zones de transfert dans les chaînes plissées: géométrie, conditions de formation et pièges structuraux associés. Unpublished PhD thesis, Chambéry (Savoie, France).

Philippe, Y., Coletta, B., Deville, E., Mascle, A., 1996. The Jura fold-and-thrust belt: a kinematic model based on map-balancing. In: Ziegler, P.A, Horvath, F (Eds.), Peri-Tethys Memoir 2: Structure and Prospects of Alpine Basins and Forelands (special issue). Mémoire de Musée National Histoire Naturel 170, 235–261.

Platt, J.P., Behrmann, J.H., Cunningham, P.C., Dewey, J.F., Helman, M., Parisch, M., Shepley, M.G., Wallis, S., Weston, P.J., 1989. Kinematics of the Alpine arc and the motion history of Adria. Nature 337, 158–161.

Plessmann, W., 1972. Horizontal-Stylolithen im französisch–schweizerischen Tafel-und-faltenjura und ihre Einpassung in den regionalen Rahmen. Geologische Rundschau 61, 332–347.

Ries, A.C., Shackleton, F.R.S., 1976. Patterns of strain variation in arcuate fold belts. Philosophical Transactions of the Royal Society of London A283, 281–287.

Sanderson, D.J., Marchini, W.R.D., 1984. Transpression. Journal of Structural Geology 6, 449–458.

Schlunegger, F., Burbank, D.W., Matter, A., Engesser, B., Mödden, C., 1996. Magnetostratigraphic calibration of the Oligocene to Middle Miocene (30–15 Ma) mammal biozones and depositional sequences of the Swiss Molasse Basin. Eclogae geologicae Helvetiae 89, 753–788.

Scholz, C.H., Cowie, P.A., 1990. Determination of total geologic strain from faulting. Nature 346, 837–839.

Schrader, F., 1988. Das regionale Gefüge der Drucklösungsdeformation an Geröllen im westlichen Molassebecken. Geologische Rundschau 77, 347–369.

Schreurs, G., 1994. Experiments on strike-slip faulting and block rotation. Geology 22, 567–570.

Sheffels, B.M., 1995. Is the bend in the Bolivian Andes an orocline? AAPG memoir 62, 511–522.

Sommaruga, A., 1997. Geology of the central Jura and the Molasse Basin: new insight into an evaporite-based foreland fold and thrust belt. Mémoire de la Société des Sciences naturelles de Neuchâtel 12, 145.

Sylvester, A.G., 1988. Strike-slip faults. Geological Society of America Bulletin 100, 1666–1703.

Tait, J.A., Bachtadse, V., Soffel, H., 1996. Eastern Variscan fold belt: Paleomagnetic evidence for oroclinal bending. Geology 24, 871–874.

Tschanz, X., 1990. Analyse de la déformation du Jura central entre Neuchâtel (Suisse) et Besançon (France). Eclogae geologicae Helvetiae 88, 543–558.

Tschanz, X., Sommaruga, A., 1993. Deformation associated with folding above frontal and oblique ramps around the rhomb shaped Val-de-Ruz basin (Jura Mountains). Annales Tectonicae 7, 53–70.

Wezel, F.C., 1986. The origin of arcs. In: Developments in Geotectonics, vol. 21. Elsevier, Amsterdam.

Wilkerson, M.S., Medwedeff, D.A., Marshak, S., 1991. Geometrical modeling of fault related folds: a pseudo-three-dimensional approach. Journal of Structural Geology 13, 801–812.

Wilkerson, M.S., Marshak, S., Bosworth, W., 1992. Computerized tomographic analysis of displacement trajectories and three-dimensional fold geometry above oblique thrust ramps. Geology 20, 439–442.

Published in Journal of Structural Geology, 22, issue 9, 1285-1296, 2000
which should be used for any reference to this work

A model of displacement and strain for arc-shaped mountain belts applied to the Jura arc

David Hindle[a,*,1], Olivier Besson[b], Martin Burkhard[a]

[a]*Institut de Géologie, rue E. Argand 11, CP 2, CH 2007 Neuchâtel, Switzerland*
[b]*Institut de Mathématiques, rue E. Argand 11, CP 2, CH 2007 Neuchâtel, Switzerland*

Received 15 July 1999; accepted 9 March 2000

Abstract

A plan view geometric model for simple, parallel, differential displacements is presented. As an analogue for models of arcuate mountain belt formation we use the model to predict strain patterns produced by parallel displacement in front of a rigid versus deformable indenter. A rigid indenter is simulated by an irregular quadrilateral displaced a constant amount along its hinterland boundary. A deformable indenter is simulated by an irregular quadrilateral displaced along a hinterland boundary that is allowed to rotate. Some simple test cases show that the deformable indenter model leads to a pattern of strain very similar to that encountered in arcuate mountain belts. Short axes orientations are most deviated from the transport direction along the lateral edges of the model with minimum displacement and shortening and vary across the central domain, mirroring strain features with variable orientations from mountain belts such as fold trends and minor deformation features such as horizontal stylolite peaks. The rigid indenter model also generates short axes deviated from the transport direction but showing far less variation. Displacement–strain relationships from the Jura mountains (Switzerland and France) are quantified based upon a simplified version of the finite displacement field for the Jura fold–thrust belt of Philippe, Y. (1995) [''Rampes latérales et zones de transfer dans le chaines plissées''. (Unpublished PhD thesis, Université de Savoie)]. We find that the model short axis orientation pattern is very similar over at least the eastern and central Jura to the stylolite patterns from the region whilst the long axes closely match the fold axes trends. The model suggests that the Jura mountains could have formed as a result of a progressive deformation with uniform transport in a general northwest direction.

1. Introduction

The form of arcuate fold and thrust belts has long fascinated geologists (Argand, 1922; Carey, 1955; Ries and Shackleton, 1976; Marshak, 1988; Ferrill and Groshong, 1993). Intuitive interpretations of a curved mountain belt suggest the need for radial movement of material to produce the curved fold axis patterns we witness (Argand, 1922; Carey, 1955). Radial displacement of any form will immediately create a space problem for the material in the arc which will have to 'stretch' drastically to accommodate the movement (Ferrill and Groshong, 1993). Restoring such a system could lead to all material moving back to a single point—a source-sink. Evidence for the large strike parallel extensions required by such a mechanism is lacking. More careful consideration of the problem has led to the conclusion that material constrained to move in a uniform direction can create strongly curved fold patterns (Ries and Shackleton, 1976; Ferrill and Groshong, 1993). Such differential shear models have, up until now, focused on distinguishing fold–thrust belt curvature forming mechanisms. These studies particularly emphasised the importance of the pattern of tangential elongation as the key parameter for dis-

* Corresponding author. Tel.: +49-331-288-1313; fax: +49-331-288-1370.
E-mail address: hindle@gfz-potsdam.de (D. Hindle).
[1] Now at: GeoForschungsZentrum Potsdam, Projektbereich 3.1 Telegrafenberg C223, D-14473 Potsdam, Germany

tinguishing between curve forming mechanisms (e.g. transport parallel simple shear, radial thrusting, pure bending, etc.). There has also been some confusion over what are the possible arc geometries resulting from different variants of differential shear. Displacement–strain relationships have sometimes been drawn intuitively, and incorrectly. For instance, both Ries and Shackleton (1976) and Marshak (1988) suggested that uniformly shortened regions with boundaries that are not orthogonal to transport direction would have fold axes orthogonal to the transport direction. This is shown (see Fig. 2, model 1) to be untrue. Often relationships between displacement and strain are counter-intuitive, and only a mathematical derivation of the strain pattern from the displacement field is sure to give correct results. This is an extension of the relationship between displacement and strain of which geologists have long been aware (Howard, 1968; Means, 1976; Ramsay, 1976).

If we accept differential shear as a mechanism for arc formation, two model classes can be distinguished based on what happens not in the thrust belt itself, but in the region indenting it. These follow from the work of Hindle and Burkhard (1999) which clarifies the fundamental differences between many proposed arc formation models. We only produce models of the 'Primary arc' type defined by Hindle and Burkhard (1999) and give more precise numerical data on the effects of deformation and its relationship to different displacement geometries. The aim is to try and identify which model is the most plausible for forming arcs. Therefore, we demonstrate the rationale of displacement–strain models for very simple, geometric analogues to arcuate fold and thrust belts and then compare these models to a real example: the Jura arc, part of the western alpine collisional system.

The Jura mountains are the latest (Middle Miocene onward) and most external part of the northwestern alpine deformation zone (Sommaruga, 1999). They are a small (ca. 350 km long) arcuate (the trend of the mountains varies by 90° along their length), fold and thrust belt, varying in width from 0 km at the eastern end to around 65 km in their central portion. They have been interpreted as being both a thick-skinned fold and thrust belt with various basement structures thought to be involved in their evolution [e.g. wrench faulting in the basement folding the cover above (Pavoni, 1961), penetration of basement thrusts into the cover (Aubert, 1945), crustal delamination due to a shallow dipping basement thrust soling out in the crust (Ziegler, 1982)] or a thin-skinned, allochthonous belt, with the Mesozoic cover shortened above an evaporite detachment regionally present within the Triassic (Schardt, 1906; Schardt, 1908; Buxtorf, 1916; Burkhard, 1990; Sommaruga, 1995; Burkhard and Sommaruga, 1998; Sommaruga, 1999). Most recently, these ideas have been based on regional interpretation of industry seismic lines across the Swiss Molasse Basin and Jura which are now publicly available. When combined with balancing arguments, the autochthonous, thin-skinned interpretation for the Jura mountains is the most reasonable. We base all our modelling on a thin-skinned interpretation. The results of our modelling show that the fold axes trends and orientation of horizontal stylolite peaks (regional strain markers for the Jura) can be simulated by the long and short axes produced by a model of differential shortening with uniform transport direction.

2. A simple, geometric, displacement–strain model

2.1. Model characteristics

In order to show the effect of displacement of material seen in plan view on the strain pattern within that material we adopt a geometric approach. Mechanical properties of rocks are considered isotropic and homogeneous. A starting point for a model is a quadrilateral. This geometry was used before by Ferrill and Groshong (1993) describing the parallel displacement of material across the length of arcuate fold belts.

With suitable mathematical manipulation (see Appendix A), we can use any quadrilateral form we

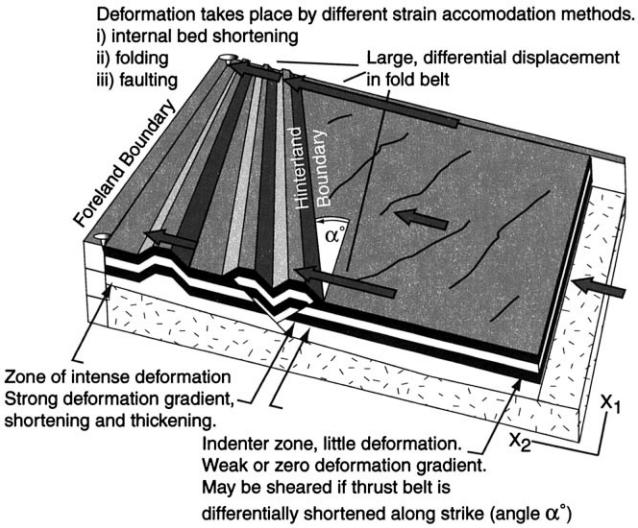

Fig. 1. A hypothetical fold and thrust belt illustrating the idea of a displacement gradient. In the picture above, there are gradients in the transport direction, which is considered to be unique, and also along strike of the mountain belt, since there is a differential displacement in this direction. The diagram makes a clear separation between an indenter region undergoing passive transport but also lightly deformed by shearing, pushing into a mountain belt which is strongly differentially shortened along strike and which deforms by thrusting and folding. Displacement drops to zero across the width of the fold belt (shown by 'pins') creating a displacement gradient orthogonal in the X_2 direction.

wish. However, to create a parallel displacement field, the corners must move in a parallel direction. The behaviour of an indenting region to an arcuate fold and thrust belt is also of considerable interest in these problems. The indenter and thrust belt are joined to each other (see Fig. 1), and any movement of their common boundary must also be present in the indenting region. Consequently, if the common boundary twists or rotates, this component of movement will be present in the indenter too, and should be reflected in the deformation pattern found there. If there is no twist or rotation, but simply a constant translation of the boundary, it is possible that the indenter will behave as a rigid block and show very little deformation. Burkhard (1990) discussed some of the different possible arc-indenter configurations in the context

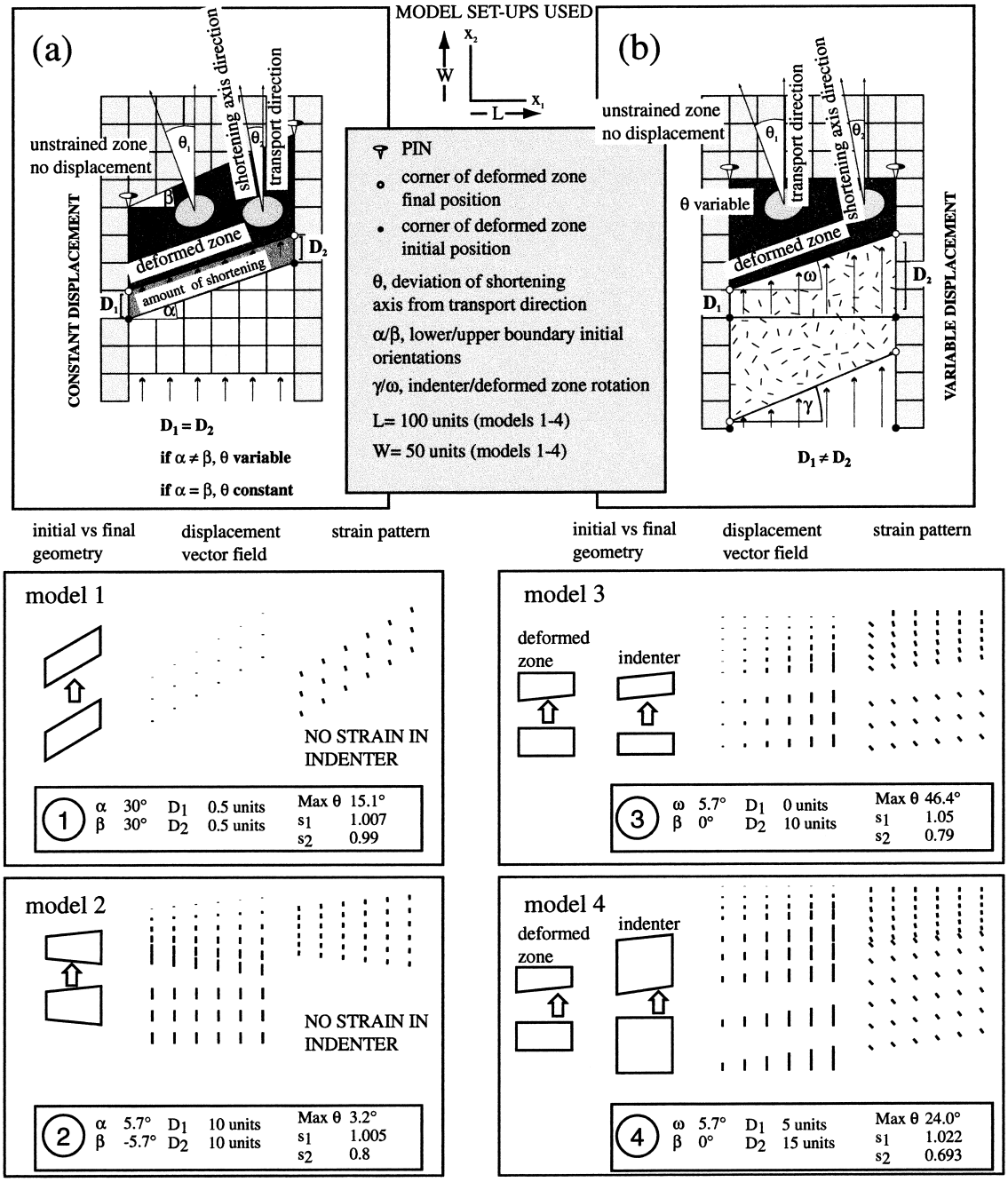

Fig. 2. Illustrative models for deformation patterns generated by transport parallel simple shear. Two types of model are used, (a) shows a 'rigid indenter' and (b) shows a deformed indenter. Model results numbered 1–4 are presented which show graphical plots of both displacement vectors and shortening axes (in their correct orientation) shown to scale and summarise the boundary conditions (α, β, γ, ω, D) and the resulting maximum values of shortening and lengthening (s_3 and s_1) and maximum angle (θ) between s_3 and the transport direction in smaller numbered boxes.

of the Jura arc and identified four models for the indenter, all variants of deformed or undeformed indenters. These broad categories provide useful boundary conditions for the models. A rigid indenter neatly translates into constant displacement of material along the thrust belt/indenter limit, whilst a deformable indenter allows variable displacement along this boundary. We apply the additional constraint of material always moving parallel, and produce four illustrative models, two with an 'undeformed indenter', two with a 'deformed indenter'.

The rigid indenter models (Fig. 2a, and models 1 and 2) have deformed zone boundaries which are oblique to the transport direction of the rigid indenter. The common indenter/deformed zone boundary moves by a constant amount along its width ($D_1 = D_2$). The same movement distance is applied to every point in the indenter, which undergoes a rigid body translation. Within the deformed zone, the displacement decreases smoothly to zero by the foreland edge of the deformed zone, generating a displacement gradient in the direction of transport. The models vary by changing the inclinations of the foreland and indenter/fold belt boundaries, producing homogeneous ($\alpha = \beta$) or inhomogeneous ($\alpha \neq \beta$) deformation.

Such models were seen as analogous to arc forming mechanisms by many authors (Carey, 1955; Ries and Shackleton, 1976; Marshak, 1988). They are a direct analogue to model B of Burkhard (1990), for the Molasse–Jura system where a rigid Molasse Basin pushes east–west, obliquely into the Jura mountains.

The deformable indenter models (Fig. 2b) have a deformed region/indenter common boundary undergoing a rotation (angle ω), which also affects material in the indenter region. The indenting region may have a hinterland boundary undergoing a different rotation (γ). The indenter region is deformed as a result. The 'thrust belt' itself will be inhomogeneously deformed as the model is set up with a fixed foreland boundary and a rotated boundary common with the indenter. The two models presented have similar characteristics to the transport parallel simple shear idea of Ferrill and Groshong (1993).

2.2. Mathematical principle

The quantity known as the displacement gradient is the key to the following models. Displacement gradient refers to changes in the total displacement of points between the original state and the deformed state along a particular direction. Hence, we could define such a quantity along only one coordinate axis, and have effectively a one-dimensional quantity, or we could envisage it existing in all directions in a plane, and have a fully two-dimensional quantity, shown conceptually in Fig. 1. The idea is thoroughly dealt with by Means (1976).

In our analysis of fold–thrust belt curvature formation, we make a distinction between the indenter zone and the fold–thrust belt itself (Fig. 1). The two regions are joined and continuous but there is a jump in the displacement gradient between them. The displacement vectors in the thrust belt diminish in magnitude in the transport direction, reaching zero along the outer boundary of the thrust belt. There is a consequential horizontal shortening (and would be a vertical thickening) of the crust to accommodate the differential movement, which occurs through folding and faulting. The indenter undergoes the full movement of the most translated part of the fold–thrust belt, but all parts of the indenter move (approximately) the same distance in the transport direction at least, and hence the displacement gradient and consequently deformation, is very small.

A gradient orthogonal to the transport direction may also develop, resulting in transport parallel differential displacement (or what one may term differential shear). As the fold–thrust belt is pinned (see Fig. 1) along an arbitrary foreland boundary, all displacement of material reaches zero along this line. If any point of the indenter region moves further into the fold–thrust belt than adjacent points, there is a differential shortening in the fold–thrust belt itself according to the position in a direction orthogonal to material transport vectors for the thrust belt. This can be seen in Fig. 1, where displacement vectors have different lengths along this direction. The consequence of transport parallel differential displacement is a transport parallel, differential shear which produces a variable strain pattern in the region. We note (see Fig. 1) that in many thin-skinned mountain belts, horizontal movement of material is often more than an order of magnitude greater than vertical. In this paper we think particularly of the Jura arc, where horizontal shortening of 25–30 km is likely whilst relief due to thrusting is restricted to 1–2 km. Hence we can justify modelling displacement and strain in the horizontal plane only (i.e. in map view) and the problem reduces to two dimensions.

The displacement gradient can be described by a coordinate transformation matrix from which we derive the finite-strain tensor for the region. In a simple quadrilateral for instance, there is a relationship between the displacement gradient matrix $\mathbf{F}$, and the components of the individual displacement vectors affecting each of the quadrilateral corner points $\mathbf{P}_n$ (n = 1–4) which is demonstrated fully in the Appendix A. If we calculate this, we have a simple model for plan view strain. We use a quadrilateral domain since this evaluates a continuous function for strain across

its domain, equivalent to 'averaging' the displacement field due to folding, faulting, etc.

3. Model results

We have used four general models, two for undeformed indenters, and two for deformed indenters. They all have uniquely parallel material displacement vectors (assumed to be parallel to the X_2 axis of a general, Cartesian co-ordinate system) and yet all have short axes which are deviated from the transport direction. The degree of deviation varies according to the boundary conditions used. However, any model with a rotational boundary (indenter/fold belt common boundary) generally shows the strongest variability of orientation of short axes. In all models including those with constant boundary displacements we find differential displacements are generated along any line parallel to the X_1 axis and there are displacement gradients in all directions in the model plane. This occurs in spite of the uniquely parallel movement of material. The general model characteristics and specific results are laid out in Fig. 2.

3.1. Model 1

Model 1 involves constant displacement applied to a region of uniform width which is oblique to transport direction. It is a case previously considered by Sanderson and Marchini (1984). He recognised that even though shortening across a region is constant, if the transport is oblique to the region and even if it has a 'symmetrical' geometry (parallelogram) a differential displacement is generated. The result is a uniform directed θ (homogeneous deformation) differing from the transport direction (15°). The angle θ will vary as a function of both the obliquity of a region to transport and the amount of shortening.

3.2. Model 2

In model 2, a rigid indenter pushes into a zone of variable width and geometry, with both boundaries inclined to the transport direction ($\alpha = -5.7°$, $\beta = 5.7°$ measured from X_1). The resulting deformation is symmetric about the median line of the deformed zone, and is inhomogeneous. There are only tiny variations in the angle θ. The largest difference between the short axis and the X_2 axis is 3.2°. In the direction of maximum stretch, there is hardly any lengthening ($s_1 = 1.005$ maximum). This small difference in orientation of shortening axes reflects the very weak differential displacement along strike in the model.

3.3. Model 3

In model 3, we represent a deformable indenter, since the common indenter/deformed zone boundary undergoes rotation. This is a composite model of an arc and its indenter. The deformed zone is initially rectangular in shape, the common indenter/deformed zone boundary undergoing a zero displacement at its left extremity, and a maximum displacement at its right extremity (rotation, $\omega = 5.7°$). This produces an inhomogeneous deformation in the deformed zone, as there is no movement of the foreland boundary. To accommodate the movement, the indenter behind the deformed zone must also be sheared. In this case, both a homogeneous simple shear and shortening is applied to the indenter, which undergoes a small shortening and an equal rotation (= simple shear) of its foreland and hinterland boundaries. Deviations of shortening axes from the X_2 direction are far greater with this configuration. Maximum deviation occurs along the left-hand (unshortened) edge, where the state of strain is simple shear only. The remainder of the deformed zone is increasingly shortened resulting in lower angular deviations. A surprising consequence of this model is the 0° deviation of shortening axes along the upper boundary where the state of strain is pure shear only. This implies an instantaneous passage at some point from $\theta > 45$–0°. Assuming fold axes perpendicular to the local direction of s_3, the model would produce a series of curved folds becoming progressively more parallel to X_1 in the positive X_1 direction (similarly along X_2). There is also considerably more (up to 1.05) extension in the direction of the long axis.

3.4. Model 4

Model 4 contains the following important features. The deformed zone is shortened by a translational component of the common indenter/deformed zone boundary, in addition to a differential displacement of this boundary along strike. The indenter region also undergoes a differential shortening along strike. It is sheared to accommodate the displacements in the deformed zone, however, its hinterland boundary rotates more than its foreland boundary, creating differential shear ($\gamma = 8.5°$). Moreover, a small shortening component is applied to the whole zone (less than that applied to the deformed zone). Every point in the indenter has an additional translation applied to it. The translation is of the same amount as the additional shortening applied to the deformed zone. The indenter thus configured has a strain pattern with the deviation of shortening axes from X_2 decreasing in both positive X_1 and X_2 senses. The result of additional shortening in the fold-belt region of the model is to reduce the deviation of shortening axes from the

X_2 direction (compare to results for model 3 for instance).

4. Discussion

The model results demonstrate how differential shear in a deformed region leads to strains which are highly variable in both orientation (θ) and magnitude (stretches, s_1—maximum extension and s_2—maximum shortening). Differential shear is generated by both uniform displacement of the lower boundary to an irregularly shaped region or by rotation of a lower boundary of a regular or irregular region. Rotations cause large differential shear and consequently larger maximum θ and s_1/s_2. Any general, additional shortening across the region ($D_1 > 0$), leads to a reduction in maximum θ (see difference between models 2 and 3).

The geometries shown are scale independent and analogous to many geological situations. In arcuate mountain belts, we may examine the relationship between fold-axis orientations and other finite-strain markers such as stylolites or calcite twins, and transport direction of material in the region. We may assume predicted θ to be locally parallel to stylolite teeth and at 90° to fold axes. The conclusion would be that a configuration such as model 2 would resemble an arcuate mountain belt in many ways. However, this is slightly unrealistic since in a mountain belt, at such high strains, a large amount of displacement is taken up by faulting.

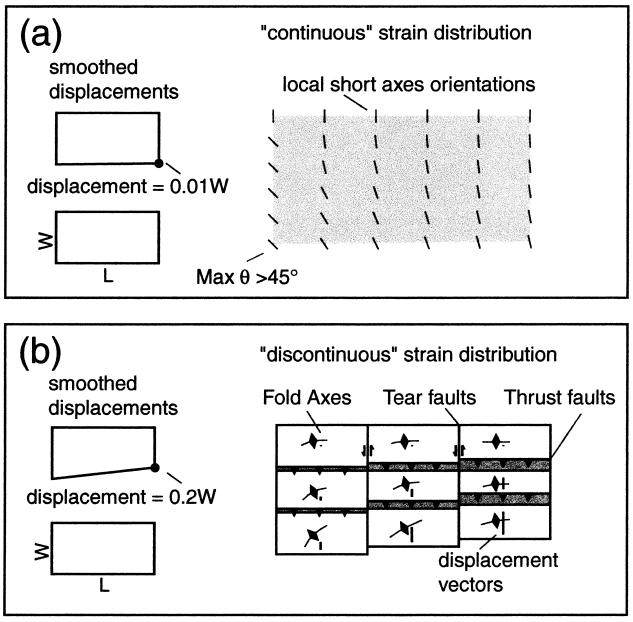

Fig. 3. Finite strain accumulates in small increments but the geometry of each increment may remain relatively constant over time. Small deformation features form from the onset of deformation whilst large-scale ones (faults and folds) form after many increments. (a) shows a tiny increment of transport parallel differential shear. The resulting fanning strain pattern has $\theta > 45°$ along one lateral edge of the model and $\theta \approx 0°$ along the opposite edge. Early strain features like stylolites should exhibit this sort of strain pattern too. (b) shows a larger amount of transport parallel differential shear, which could be thought of as resulting from 200 increments of (a). Deformation mechanisms change to accommodate the larger strain (shown schematically). Once faulting has begun, most new deformation will accumulate on faults, and the system will behave as a series of differentially translated, semi-rigid blocks. However, earlier-formed, low-deformation features would be present within these blocks and may preserve their original orientations.

Indeed, all the deformation accumulated by different mechanisms in a thin-skinned thrust belt can be thought of as accommodating some regional scale strain. The important thing to remember is the progressive nature of the deformation. Features such as stylolites and possibly some heterogeneities provoking early folding would begin forming in the very earliest stages of deformation of a region (Fig. 3a) when total strain is very low. This initial geometry of deformation may still be similar to that seen at the end of the episode. Indeed, the total finite deformation for transport parallel simple shear could be thought of as accumulating by a succession of increments such as in Fig. 3(a). Taking a similar rectangular domain as we have used for our first strain models, we apply a tiny displacement to one of its corners (Fig. 3a) and simulate one such increment. We see that even the smallest differential shear will give $\theta > 45°$. If this is the deformation geometry affecting an arcuate mountain belt, we would expect early strain features such as stylolites to form with orientations similar to predicted θ. Some early folding (and possibly faulting) could also be initiated in the same orientation. Further deformation (Fig. 3b) would be accommodated by faulting and folding, and may occur by translation of discrete, semi-rigid blocks. However, already formed folds and stylolites would keep their early orientations, which might be rotated passively if the differential shear continues.

Therefore, though the detailed processes governing formation of strain features are complicated, the orientations and patterns we find should be related to the geometry of deformation applied. Our modelling simulates the average or total strain applied to a region which may be accommodated by a number of mechanisms. Reches (1978) also suggested that groups of faults act together to accommodate regional strains and their orientation would have a clear relationship to the regional scale strain field that was developing. Even for simple homogeneous strains, four differently oriented fault planes would exist. Molnar (1983) suggested an inverse process where earthquake magnitudes on differently oriented faults could be summed to give an average regional strain. Both point to the fact that faults (and folds and intergranular defor-

mation) are allowing change of shape of a large region. We argue that at the scale of a whole mountain belt, an overall deformation geometry exists and this is the key to the regional strain pattern we find.

5. The Jura Arc example

Taking these arguments further requires a real example. The Jura fold-and-thrust belt is an arcuate region of more than 350 km lateral extent, lying northwest of the northern alpine foreland basin (Swiss Molasse). The belt is composed of thrust Mesozoic strata detached from a Permo-Carboniferous 'basement' by Triassic evaporite layers. Lateral thickness variations and pinch-outs of the Triassic 'Muschelkalk' and 'Keuper' series are a major control on displacement and shortening of the cover sequence over the width of the chain and its arcuate form (Debrand Passard et al., 1984; Philippe, 1994). Following Sommaruga (1996), the mechanical behaviour of the Jura strata can be broadly characterised as follows (see Fig. 4): limestone-dominated lithologies are generally strong and brittle; shale- and marl-dominated lithologies are weaker and may be either plastic or brittle according to associated temperature, fluid pressure and relative amount and type of clay; evaporite-dominated lithologies are weak, and generally plastic. Hence, the lowermost, salt-gypsum-dominated Triassic units of the Jura are mechanically by far the weakest, and form the principal basal décollement, whilst the Upper Malm, a thick, limestone unit is by contrast very strong and has deformed under a brittle regime across much of the belt to produce the fold–thrust system we see today. The Jura mountains contain remnants of the Tertiary foreland basin Molasse sequence proving that the foreland basin's foredeep unconformity

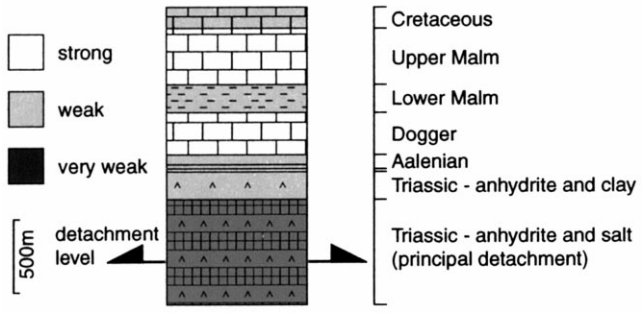

Fig. 4. Mechanical stratigraphy for the Jura mountains, adapted from Sommaruga (1996). Thicknesses shown are correct for the central Jura mountains, but vary across the chain as described in the text. The main décollement layer is illustrated by thrust arrows, and the approximate relative strengths of the lithologies are shown according to the shading of the units.

extended into the chain before it was formed. In the alpine foreland basin, hinterland to the Jura, the same Mesozoic layers dip below Molasse sediments up to 3 km thick at the alpine front. The entire wedge of Molasse and Mesozoic material remains relatively undeformed. Contractional deformation of the Mesozoic sequences in the Jura mountains develops from the post-Middle Miocene (Serravallian), onwards (Burkhard and Sommaruga, 1998).

Previous models of curvature formation in the Jura belt can be summarised according to two types of approach used. The first are based on two-dimensional, plan view restorations of the Jura (or parts of it). Hence, Laubscher (1961) originally formulated a model involving rotation of the Molasse/Jura limit, by 7° in the eastern part of the Jura mountains, constrained by the variations in shortening estimated along the strike of the belt from two-dimensional restoration. This model implies that the Jura mountains are then indented by a Molasse region which would also have been sheared. More recently, Philippe (1995) produced the most complete two-dimensional restoration of the Jura belt yet. The displacement field he derived relative to a pin line in the stable European foreland to the Jura shows an explicit rotation of the Jura/Molasse boundary, which could also mean that the Molasse Basin is a deformed (sheared) indenter. The second group of interpretations are based on static models for stress patterns suggested by different strain features found in the present-day Jura belt. Laubscher (1972) for instance, suggested a conceptually different model for curvature formation where the indenting block was effectively the western Alps (Helvetic and Prealpine nappes) pushing as a rigid block into the Molasse and Jura (i.e. both are indented but only the Jura shows significant deformation). This interpretation was chosen because the (instantaneous) stress pattern generated by such a rigid block pushing into a deformable hinterland would resemble a pattern of stress trajectories related to the variable orientation of the fold axes across the belt. Homberg et al. (1999) have recently proposed a modified indenter model in which the Molasse Basin is the direct indenter to the Jura arc; furthermore, Homberg proposes that this indenter would have broadened over time. The broadening is used as an explanation for two differing orientations of stress axes determined from sets of Mio-Pliocene fault slickenslides which pre- or post-date folding in the Jura.

The difference between the two approaches is manifest. The first, by attempting to unravel the displacements which produced the structures found in the Jura will, if carried out correctly, restore the positions of the Jura/Molasse boundary to its original position before deformation. If this limit changes shape (e.g. twists) between the undeformed and deformed states,

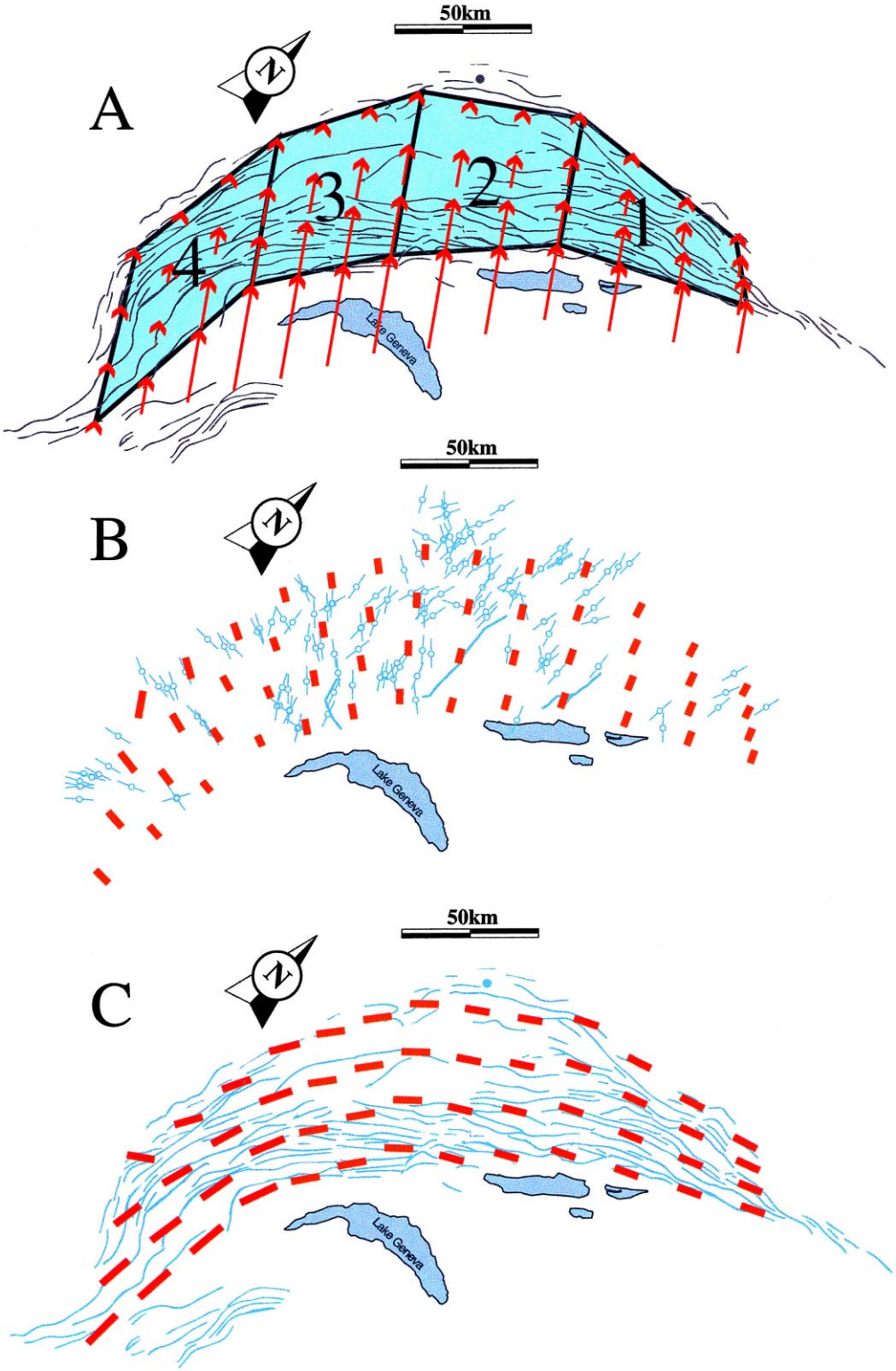

Fig. 5. Modelling the Jura using four quadrilateral domains. (a) The displacement field of Philippe (1995) is simplified to four points on the Jura/Molasse boundary, displaced differentially, in an identical direction. Jura/foreland boundary is fixed relative to these points. Four quadrilateral domains model the boundary conditions, and displacements (red vectors) are smoothly interpolated across them. Note that here, we pass from a reference element (rectangular) to two different deformed elements as outlined in the Appendix A. (b) Short axes calculated for the displacement field (red) compared to horizontal stylolites from the Jura (blue). (c) Long axes calculated for the displacement field (red) compared to fold axes from the Jura (blue).

the Molasse Basin must also have been internally deformed. The second approach attempts to find a model based upon analyses which are related to an instantaneous state of stress. As such, they ignore the large differential displacements along strike of the mountain belt accumulating over time. The arguments related to stress states are correct but do not take account of the dynamic evolution of the system over time.

We have adopted the results of Philippe (1995) and modified them slightly to model the total finite strain for the displacement field generated by two-dimensional plan view restoration of the Jura belt. Our model is simplified because rather than allowing a slight divergence of displacement vectors, we take only the displacements of four points along the Jura/Molasse boundary, and constrain them to be parallel (in an approximately northwest direction). We then pin the Jura/foreland boundary. Finally, as we model 'total' finite strain by such a technique, i.e. strain from displacement (in reality due to cumulative faulting and folding), we interpolate the displacements to decrease linearly to zero along the Jura/foreland boundary, from the values given along the Jura/Molasse boundary. These values are close to 30 km shortening (maximum) along the central and western Jura boundaries, but decline to zero at both the western and eastern Jura culminations. We substitute a continuous displacement function for what is in nature discontinuous and calculate a cumulative finite strain pattern for the Jura mountains, based on the sum of all displacement during their history. We compare the model strain data with observed strain features such as folds and horizontal stylolite peaks. The four points of known displacement are actually simulated by using quadrilateral domains as in the illustrative models.

Our results give directional information for short and long axes of the total finite strain ellipses predicted across the Jura. A rigidly parallel displacement field (Fig. 5a) produces a fanning strain pattern (Fig. 5) across a modelled Jura arc. Comparison with field data shows predicted short axes not fanning as strongly as stylolite teeth (Fig. 5b), with angular deviations of approximately 45° between measured and calculated values at the eastern and western terminations of the Jura. Predicted long axes orientations (Fig. 5c) match those of Jura folds across most of the eastern and central Jura with deviations of $< 10°$. Calculated strain axes swing by 73° in orientation across the model, which we may compare to the often-quoted 90° swing in orientation of the Jura structural grain along strike.

There are probable mechanical reasons for the difference in correspondence between the large, cumulative finite strains and different natural features. In the case of the stylolites, as already discussed (Fig. 3a), small deformations produce a widely fanning strain pattern, and since deformation is small, this would correspond closely to local principal stress trajectories. We also notice two contrasting orientations of stylolites in some places in the Jura. This has been interpreted as corresponding to two different regional stress fields. Other kinematic indicators (e.g. fault slickenslide analysis cf. Homberg et al. (1999)) also show these two trends. Such instantaneous measures of stress (or tiny strain) are not directly comparable to total finite strains. The fanning pattern is present for both model and natural data. However, deviations from transport direction are always lower in the case of the model where total shortening is large. The additional shortening component tends to pull strain axes closer into line with transport direction. Fold axes by contrast are far larger scale features and form over the course of the total deformation history of the mountain belt. The model is in very close correspondence with fold axes trends, since we compare the model to a quantity more representative of cumulative finite strain. This admittedly only offers a qualitative explanation, and the precise mechanics of the processes involved are far more complicated. Nevertheless, the likely overall geometry of total finite displacement in the Jura even when constrained to be rigorously parallel everywhere, produces the divergent pattern of strain we see in the Jura arc. It may be invoked as a mechanism for generating the arcuate geometry of the whole belt. There is no requirement of divergent transport along strike or secondary bending.

6. Conclusions

1. Illustrative models of transport parallel shear have shown any region inclined to transport direction undergoing constant displacement of one boundary will develop a fanning strain pattern, divergent from the transport direction.
2. If a region's width varies along strike and its boundary is moved a constant amount (even if the boundary is orthogonal to the transport direction) the shortening is consumed differentially along strike, generating a differential shear and again giving a fanning strain pattern, divergent from the transport direction. However, the degree of divergence for such a case is normally very small.
3. When a boundary of a region is displaced differentially along strike, the resulting fanning strain pattern is very clear, and shows strongest divergence from the transport direction along the line for which shortening in the model is a minimum. When shortening is zero along one line in such a model, the predicted strain axes along this line will diverge

by at least 45° from transport direction.

4. In general, these models illustrate that differential, parallel displacements of material in a region will generate fanning strain patterns.
5. A model of the Jura arc, allowing only parallel displacements and variable amounts of differential displacement and shortening along strike produces a fanning strain pattern across the width of the model region.
6. The orientations of stylolite teeth measured in the Jura (and also other kinematic indicators, e.g. fault slickenslides) show a similar fanning pattern but a stronger deviation from an assumed transport direction. Local angular differences of ca. 45° in orientation are found. Discrepancies most probably stem from modelling large, finite strains, and comparing them to features probably developed at a much earlier stage (lower strain) cf. point 3.
7. Fold axes trends, a measure of the 'structural grain' of the Jura arc, show a very close match to the orientations of modelled, long axes of finite strain ellipses (modelled variation along strike is 73°, change in trend of the Jura is ca. 90°). We attribute this to the fact that fold axes orientations develop over the entire deformation history of the belt, and consequently are closely related to the total calculated finite strains.
8. We conclude that geometrically constrained models of arcuate fold-and-thrust belt indentation give valuable information about the evolution of the indenter. Based on the evidence of several restorations (Laubscher, 1961; Philippe, 1995), the Molasse Basin has been deformed as it has a common boundary with the Jura arc, shown to have been rotated. Moreover, applying the finite displacements predicted by such a model generates a fanning strain pattern. Models of indentation based on stress patterns developing ahead of a rigid indenter (Laubscher, 1972; Homberg et al., 1999), predict fanning stress/strain patterns, but are instantaneous solutions to a problem. They ignore the accumulation of incremental strains over time and the changes in geometry of the system that this requires.

Acknowledgements

Very helpful reviews by David Ferrill and François Jouanne have substantially improved the scope of the manuscript. This study was supported by Swiss National Science Foundation Grants No. 20-43055.95 and 20-50535.97; it is a part of the PhD thesis of DH.

Appendix A. Mathematical derivations

Fig. A1 shows the general set up for the model. We see an initial rectangular element, $\mathbf{P}_n$ (n = 1–4), dimensions (L, W) transformed onto a general quadrilateral, $\mathbf{P}_n'$. The components of the vectors linking the two are named individually. These transformations give:

$$\mathbf{P_1} = \begin{pmatrix} 0 \\ 0 \end{pmatrix} \rightarrow \mathbf{P}_1' = \begin{pmatrix} B \\ A \end{pmatrix},$$

$$\mathbf{P}_2 = \begin{pmatrix} L \\ 0 \end{pmatrix} \rightarrow \mathbf{P}_2' = \begin{pmatrix} L+D \\ C \end{pmatrix},$$

$$\mathbf{P}_3 = \begin{pmatrix} L \\ W \end{pmatrix} \rightarrow \mathbf{P}_3' = \begin{pmatrix} L+F \\ W+E \end{pmatrix},$$

$$\mathbf{P}_4 = \begin{pmatrix} 0 \\ W \end{pmatrix} \rightarrow \mathbf{P}_4' = \begin{pmatrix} H \\ W+G \end{pmatrix}. \tag{A1}$$

We then derive four functions which individually attribute a value of 1 to one point $\mathbf{P}_n$ and simultaneously zero to all others (shape functions)

$$f_1 = (L - x_1)(W - x_2)\frac{1}{LW}$$

$$f_2 = x_1(W - x_2)\frac{1}{LW}$$

$$f_3 = x_1 x_2 \frac{1}{LW}$$

$$f_4 = (L - x_1)x_2\frac{1}{LW}. \tag{A2}$$

Now multiplying each function f_n by each new coordinate $\mathbf{P}_n'$ yields an equation of the form

$$\mathbf{x} = \sum_{n=1}^{4} f_n \mathbf{P}_n', \tag{A3}$$

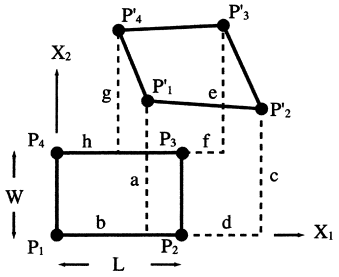

Fig. A1. Deriving transformation constants. The components a–h are shown positioned according to the equations derived in Appendix A. All models begin from a reference element with dimensions L, W as shown.

Where $\mathbf{x} = \binom{x_1}{x_2}$ is the transformed co-ordinates of a point. The resulting displacement equations take a general form

$$x_1 = a_{11}X_1 + a_{12}X_2 + a_{13}X_1X_2 + a_{14}$$

$$x_2 = a_{21}X_1 + a_{22}X_2 + a_{23}X_1X_2 + a_{24}. \quad \text{(A4)}$$

We then differentiate with respect to X_1, and X_2 in turn. This gives us the deformation gradient matrix

$$\frac{\partial x_i}{\partial X_j} = \begin{bmatrix} a_{13}X_2 + a_{11} & a_{13}X_1 + a_{12} \\ a_{23}X_2 + a_{21} & a_{23}X_1 + a_{22} \end{bmatrix} = \mathbf{F}_{ij}. \quad \text{(A5)}$$

The matrix can be used in the manner $d\mathbf{x} = \mathbf{F} \cdot d\mathbf{X}$, thereby associating a vector at initial position $\mathbf{X}$ to another vector at final position $\mathbf{x}$. This specification (sometimes called Lagrangian) refers to the undeformed configuration. We find it more relevant to work in a deformed (Eulerian) configuration, since when making field measurements, we work in deformed material and ignore its initial position. We therefore prefer a specification $d\mathbf{X} = \mathbf{F}^{-1} \cdot d\mathbf{x}$, and require the inverse of the tensor $\mathbf{F}$. Various strain and deformation tensors exist and are well presented by (Malvern, 1969) (chapter 4). We use the Cauchy deformation tensor $\mathbf{B}^{-1}$. This gives the initial squared length (dS^2) of an element $d\mathbf{x}$ identified in the deformed configuration

$$\mathbf{B}^{-1} = (\mathbf{F}^{-1})^t \cdot \mathbf{F}^{-1}. \quad \text{(A6)}$$

So, we have the general displacement equation for the rectangle onto any quadrilateral. If we wish to take a general quadrilateral as the **initial** shape and deform that, a solution is also possible. We work from an initial rectangular element—a reference element.

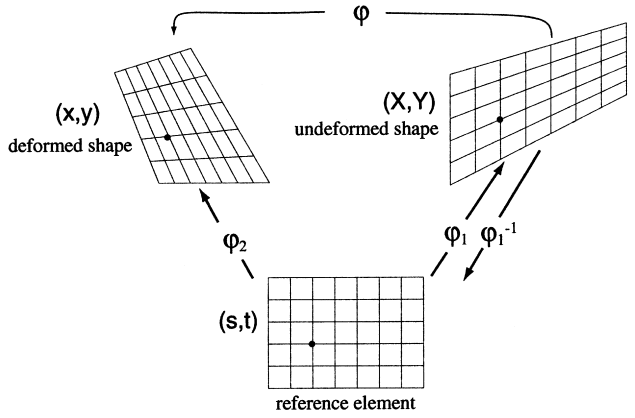

Fig. A2. Although we want a single function φ, it is easier to work from a reference element and carry out two separate transformations. We therefore work between three separate co-ordinate systems, (s, t), (X, Y), (x, y) defining the original co-ordinate grid in (s, t). Functions mentioned in the text are shown schematically.

Eqns (A4) govern the transformation of the rectangle onto **both** any initial quadrilateral and any final quadrilateral. Thus a co-ordinate point (s, t) in the reference element (Fig. A2) is associated to a point (X, Y) in the initial configuration by application φ_1 and to a point (x, y) in the final configuration by application φ_2. Both applications φ_1 and φ_2 are of the form of Eqns (A4). A global application φ can be imagined which directly associates a point (X, Y) to a point (x, y). It is equivalent to the composite function

$$\varphi_2\left(\varphi_1^{-1}(X,Y)\right) \text{ or } \varphi_2 \cdot \varphi_1. \quad \text{(A7)}$$

It is also equivalent to associating either 'end' of the equations

$$\varphi_1(s,t) = (X,Y) \text{ and } \varphi_2(s,t) = (x,y). \quad \text{(A8)}$$

By using (s, t) this way, we can effect a co-ordinate transformation of a known point in ALL co-ordinate systems, without directly knowing φ_1^{-1}. To calculate deformations, we need to know $\mathbf{D}\varphi$.

$$\mathbf{D}\varphi = \mathbf{D}\left(\varphi_2 \cdot \varphi_1^{-1}\right) = \mathbf{D}\varphi_2 \cdot \mathbf{D}\left(\varphi_1^{-1}\right) = \mathbf{D}\varphi_2 \cdot \mathbf{D}\varphi_1^{-1}. \quad \text{(A9)}$$

We need to find $\mathbf{D}\varphi^{-1}$.

$$\mathbf{D}\varphi^{-1} = \left(\mathbf{D}\varphi_2 \cdot \mathbf{D}\varphi_1^{-1}\right)^{-1} = \mathbf{D}\varphi_1 \cdot \mathbf{D}\varphi_2^{-1}. \quad \text{(A10)}$$

Then, like Eqns (A6)

$$\mathbf{B}^{-1} = \left(\mathbf{D}\varphi^{-1}\right)^t \cdot \mathbf{D}\varphi^{-1} = \left(\mathbf{D}\varphi_2^{-1}\right)^t \cdot \mathbf{D}\varphi_1^t \cdot \mathbf{D}\varphi_1^t \cdot \mathbf{D}\varphi_2^{-1}. \quad \text{(A11)}$$

References

Argand, E., 1922. La tectonique de l'Asie. In: Congrès Géologique International. Extrait du compte-rendu du XIIIe congrès géologique internationale, Brussels, pp. 171–372.

Aubert, D., 1945. Le Jura et la tectonique d'écoulement. Memoire de la Société Vaudoise des Sciences Naturelles 12, 93–152.

Burkhard, M., 1990. Aspects of the large scale Miocene deformation in the most external part of the Swiss Alps (Subalpine Molasse to the Jura fold belt). Eclogae Geologicae Helvetiae 83, 559–583.

Burkhard, M., Sommaruga, A., 1998. Evolution of the Western Swiss Molasse Basin structural relations with the Alps and the Jura belt. In: Mascle, A., Puigdefabregas, C., Luterbacher, H.P., Fernandez, M. (Eds.), Cenozoic Foreland Basins of Western Europe (134). Geological Society Special Publications, London, pp. 279–298.

Buxtorf, A., 1916. Prognosen und Befunde beim Hauensteinbasis und Grenchenberg tunnel und die Bedeutung der letzteren für die Geologie der Juragebirges. Verh. Naturforsch. Ges. Basel 27, 185–254.

Carey, S.W., 1955. The orocline concept in geotectonics. Proceedings of the Royal Society of Tasmania. 89, 255–288.

Debrand Passard, S., Courbouleix, S., Leinhardt, M.-J., 1984.

Synthèse géologique du Sud–Est de la France. Stratigraphie et Paléogéographie, Orléans.
Ferrill, D.A., Groshong, R.H., 1993. Kinematic model for the curvature of the northern Subalpine Chain, France. Journal of Structural Geology 15, 523–541.
Hindle, D., Burkhard, M., 1999. Strain, displacement and rotation associated with the formation of curvature in fold belts; the example of the Jura arc. Journal of Structural Geology 21, 1089–1101.
Homberg, C., Lacombe, O., Angelier, J., Bergerat, F., 1999. New constraints for indentation mechanisms in arcuate belts from the Jura Mountains, France. Geology 27, 827–830.
Howard, J.H., 1968. The use of transformation constants in finite homogeneous strain analysis. American Journal of Science 266, 497–506.
Laubscher, H.P., 1961. Die Fernschubhypothese der Jurafaltung. Eclogae Geologicae Helvetiae 54, 221–282.
Laubscher, H.P., 1972. Some overall aspects of Jura dynamics. American Journal of Science 272, 293–304.
Malvern, L.E., 1969. Introduction to the Mechanics of a Continuous Medium. Prentice-Hall, Englewood Cliffs, NJ.
Marshak, S., 1988. Kinematics of orocline and arc formation in thin-skinned orogens. Tectonics 7, 73–86.
Means, W.D., 1976. Stress and Strain; Basic Concepts of Continuum Mechanics for Geologists. Springer-Verlag, New York.
Molnar, P., 1983. Average regional strain due to slip on numerous faults of different orientations. Journal of Geophysical Research 88, 6430–6432.
Pavoni, N., 1961. Faltung durch Horizontalvershiebung. Eclogae Geologicae Helvetiae 54, 515–534.
Philippe, Y., 1994. Transfer zone in the Southern Jura Thrust Belt (eastern France) Geometry, development and comparison with analogue modelling experiments. In: Mascle, A. (Ed.), Hydrocarbon and Petroleum Geology of France (special issue). European Association of Petroleum Geology, pp. 327–346.
Philippe, Y. 1995. Rampes latérales et zones de transfert dans les chaines plissées. Unpublished PhD thesis, Université de Savoie.
Ramsay, J.G., 1976. Displacement and strain. In: by London, R.S.O. (Ed.), A Discussion on Natural Strain and Geological Structure. Royal Society of London, London, pp. 3–25.
Reches, Z., 1978. Analysis of faulting in three-dimensional strain field. Tectonophysics 47, 109–129.
Ries, A.C., Shackleton, R.M., 1976. Patterns of strain variations in arcuate fold belts. Philosophical Transactions of the Royal Society of London A 283, 281–288.
Sanderson, D.J., Marchini, W.R.D., 1984. Transpression. Journal of Structural Geology 6, 449–458.
Schardt, H., 1906. deux coupes générales à travers la chaîne du Jura. Archives des Sciences Physiques et Naturelles, Genève XXIII.
Schardt, H., 1908. Les causes du plissement et des chevauchements dans le Jura. Eclogae Geologicae Helvetiae X, 484–488.
Sommaruga, A., 1995. Tectonics of the Central Jura, and the Molasse Basin. New insights from the interpretation of seismic reflection data. Bulletin de la Société Neuchâteloise des Sciences Naturelles 118, 95–108.
Sommaruga, A., 1996. Geology of the central Jura and the Molasse Basin: new insight into an evaporite-based foreland fold and thrust belt. Unpublished PhD thesis, Neuchâtel.
Sommaruga, A., 1999. Décollement tectonics in the Jura foreland fold-and-thrust belt. Marine and Petroleum Geology 16, 111–134.
Ziegler, P.A., 1982. Geological Atlas of Western and Central Europe. Shell International Petroleum, Maatshappij, BV.